Supporting Information

Environment-Specific Force Field for Intrinsically Disordered and Ordered Proteins

Dong Song[1,#], Hao Liu[1,#], Ray Luo[2,*], and Hai-Feng Chen[1,3,*]
[1]State Key Laboratory of Microbial metabolism, Joint International Research Laboratory of Metabolic & Developmental Sciences, Department of Bioinformatics and Biostatistics, National Experimental Teaching Center for Life Sciences and Biotechnology, School of Life Sciences and Biotechnology, Shanghai Jiao Tong University, Shanghai, 200240, China
[2]Departments of Molecular Biology and Biochemistry, Chemical and Molecular Engineering, and Materials Science and Engineering, and Biomedical Engineering, University of California, Irvine, CA 92697-3900, USA
[3]Shanghai Center for Bioinformation Technology, Shanghai, 200235, China

*Corresponding authors
Email addresses: haifengchen@sjtu.edu.cn; ray.luo@uci.edu
Tel: 86-21-34204348
Fax: 86-21-34204348

[#]These authors contributed equally to this work.

- **Initial Investigation of Environmental Effects**

The Shi group studied the influence of neighboring residues on the J-coupling constants of the Ac-LXP-NH2 peptides. Their data show that neighboring residues play important roles in determining the stabilities of secondary structures of the central residues 'X' by influencing their hydration environments[1]. However, our investigation of widely used protein force fields, such as *ff14IDPSFF*, *ff14SB*, *a99SB-disp*, *ff03ws*, and *CHARMM36m* shows that they are not accurate enough to reproduce the reported neighboring-residue effects for these model peptides (**Figure S1**).

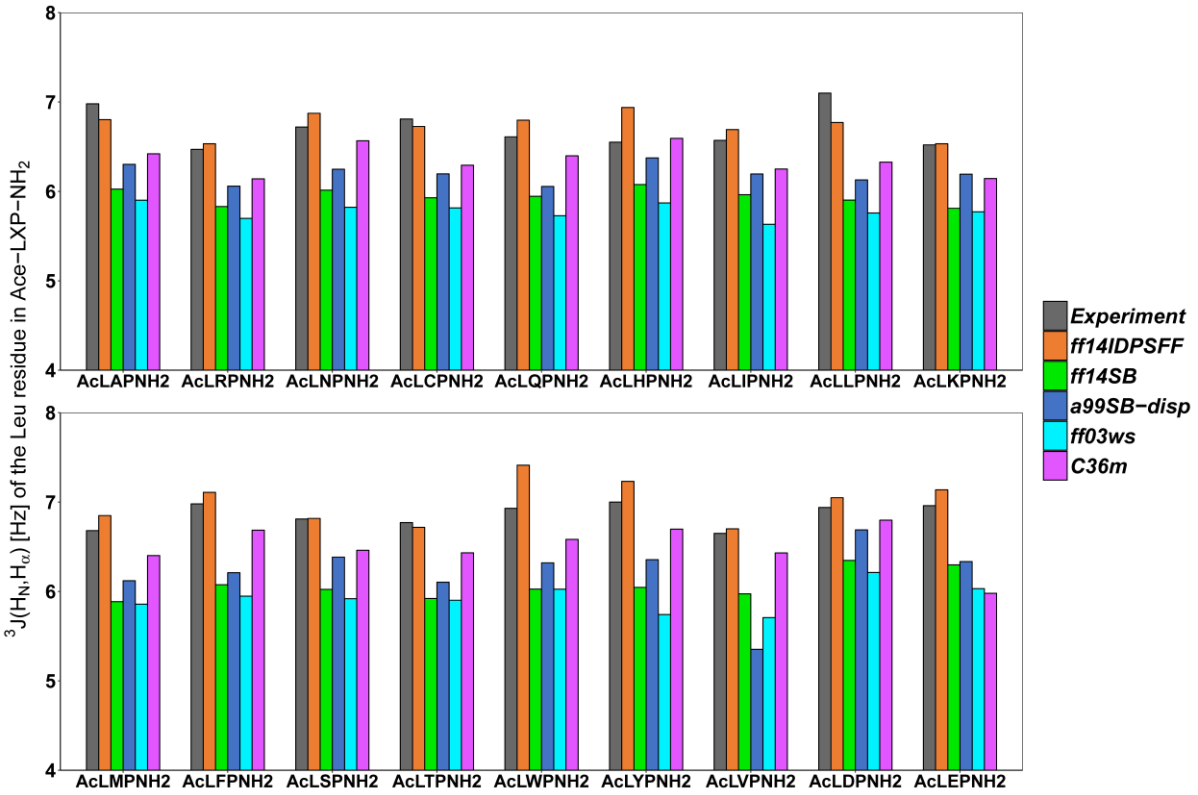

Figure S1. $^3J(H_N,H_\alpha)$ of residue Leu in Ac-LXP-NH2 from NMR experiment and MD simulation. Most force fields failed to reproduce J-couplings of the leucine adjoining different neighbor residues. *ff14IDPSFF* produces the closest $^3J(H_N,H_\alpha)$ values to experiment, though its predicted values in Ac-LQP-NH2, Ac-LHP-NH2, Ac-LWP-NH2, and Ac-LYP-NH2 are significantly higher than experiment. *ff14SB*, *a99SB-disp* and *ff03ws* underestimate the $^3J(H_N,H_\alpha)$ for all Ac-LXP-NH2. *CHARMM36m* also underestimates $^3J(H_N,H_\alpha)$ for Ac-LXP-NH2 but better than *ff14SB*, *ff99disp* and *ff03ws*, while *CHARMM36m* produces a lower $^3J(H_N,H_\alpha)$ for Ac-LEP-NH2 than other force fields.

To highlight the effect of the neighbor residues' influences on a central residue, phi/psi distributions of Gly, Pro, and other amino acids in benchmark database for each of the 4

environmental combinations are shown in **Figure S2**. It is clear that the distributions are significantly different among the 4 different environmental combinations. On the one hand, the propensity of α-left region in NP-Gly-P is significantly less than that in NP-Gly-NP, P-Gly-NP and P-Gly-P. On the other hand, the low energy connections between PPII region and α-right region for proline are totally different among NP-Pro-NP, NP-Pro-P, P-Pro-NP and P-Pro-P. For the remaining 18 amino acids, difference can also be observed in the α-right region as shown in **Figure S2**.

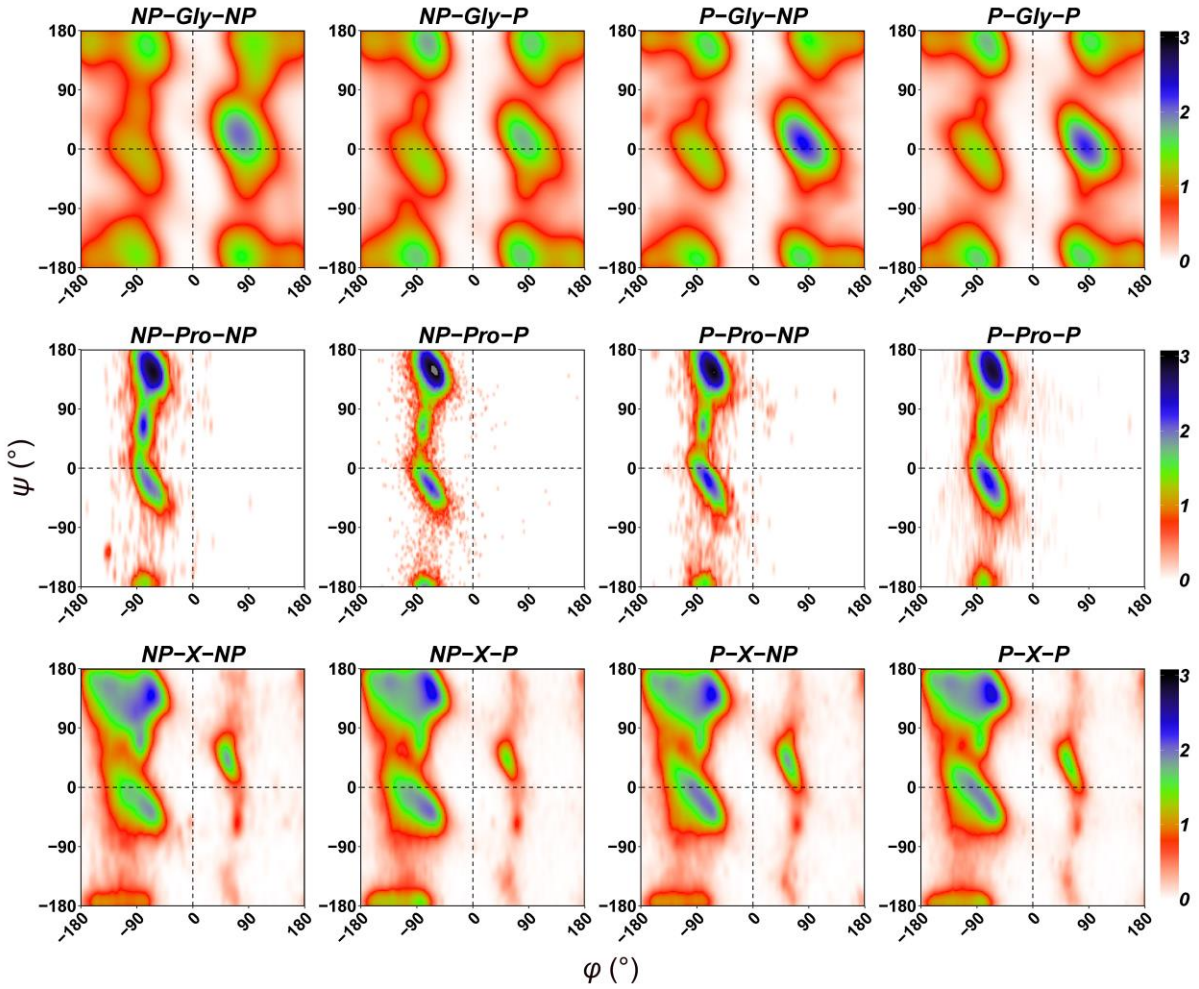

Figure S2. phi/psi distribution of Gly, Pro and other 18 residues in environmental separated benchmark phi/psi database.

Figure S3 further illustrate the populations of specific secondary structures for Ala, Leu, Ser, and Thr in the benchmark database, which also supported the finding that different neighboring environments leading to different secondary structural preferences. These initial analyses suggest that the classification of neighboring environment can provide more accurate

secondary structure propensity in MD simulations.

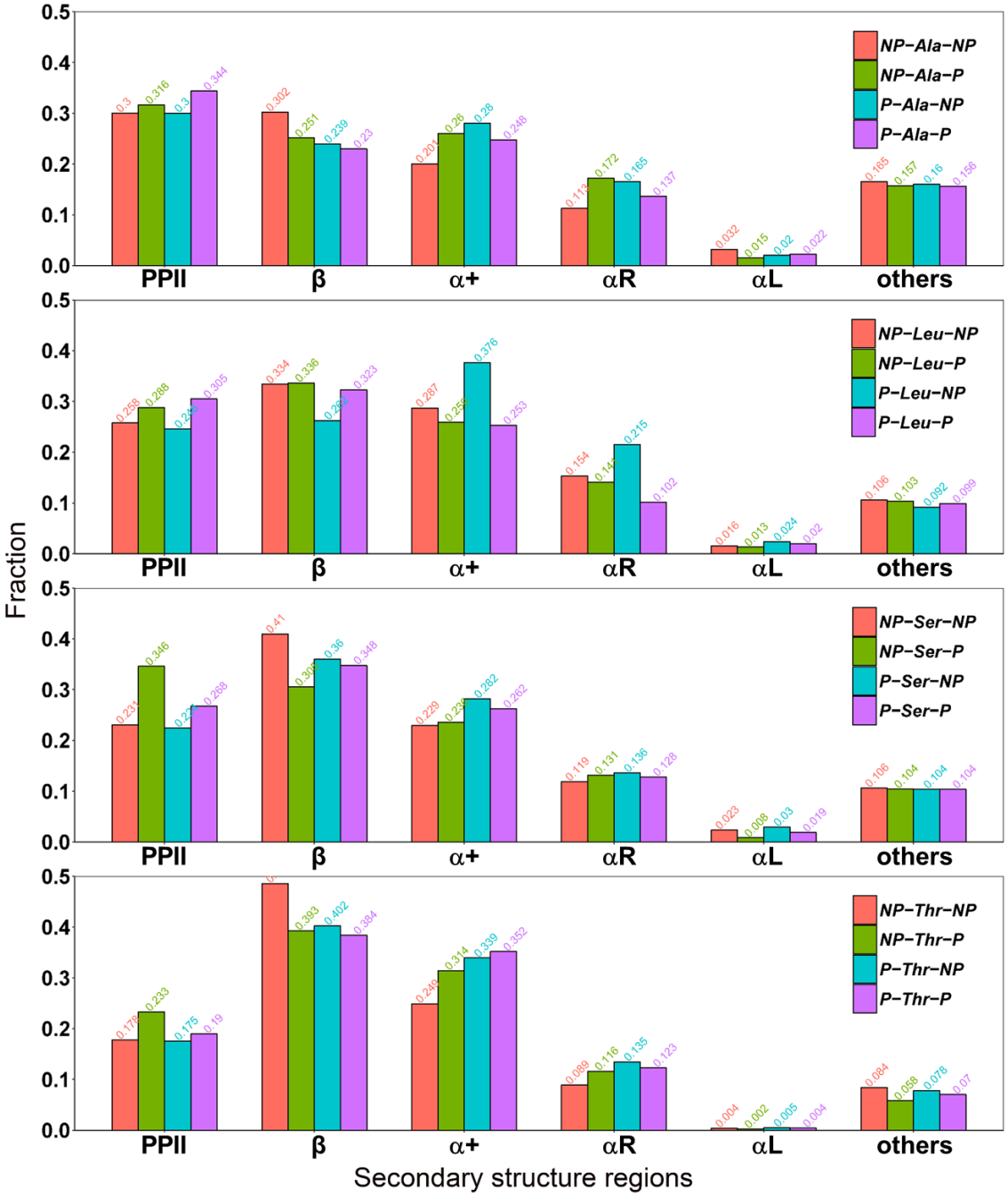

Figure S3. Propensity of different regions in Ramachandran plot for Ala, Leu, Ser, and Thr in environmental separated benchmark phi/psi database.

Table S1. Simulation conditions used in this study.

System	Force field	Length	Temperature (K)	Ionic Strength (mM)	Trajectories	Time (ns)	NMR exp.
Ac-LXP-NH_2[a]	*ff14SB, ff14IDPSFF, ESFF1, ff03ws, a99SB-disp, C36m*	3	298	0	1×18	200 (10~200)	Shi et al. [1]
GXG[b]	*ff14SB, ff14IDPSFF, ESFF1*	3	298	0	1×8	100 (20~100)	Schweitzer-Stenner et al. [2]
GGG	*ff14SB, ff14IDPSFF, ESFF1*	3	300	0	1	100 (20~100)	Schwalbe et al. [3]
VVV	*ff14SB, ff14IDPSFF, ESFF1*	3	300	0	1	100 (20~100)	Schwalbe et al.
AAA	*ff14SB, ff14IDPSFF, ESFF1*	3	275 ~ 350[c]	0	1×16	100 (20~100)	Schwalbe et al.
AAAAA	*ff14SB, ff14IDPSFF, ESFF1*	5	300	0	5	100 (50~100)	Schwalbe et al.
AAAAAAA	*ff14SB, ff14IDPSFF, ESFF1*	7	300	0	5	300 (50~300)	Schwalbe et al.
EGAAXAASS[d]	*ff14SB, ff14IDPSFF, ESFF1*	9	298	0	5×14	100 (50~100)	Grzesiek et al. [4]
HEWL19	*ff14SB, ff14IDPSFF, ESFF1*	19	293	0	5	300 (50~300)	Schwalbe et al.
TC5b (1l2y)	*ESFF1*	20	282	0	1	1000	--
villin (1vii)	*ESFF1*	36	298	150	1	1000	--
crambin (1ejg)	*ESFF1*	46	298	150	1	1000	--
LysM (1e0g)	*ESFF1*	48	298	150	1	1000	--
IgGbG (1fcl)	*ESFF1*	56	298	150	1	1000	--
BPTI (5pti)	*ESFF1*	58	298	150	1	1000	--
CSEv5 (1i6f)	*ESFF1*	60	298	150	1	1000	--
FAS1 (1fas)	*ESFF1*	61	298	150	1	1000	--
CspB (1csp)	*ESFF1*	67	298	150	1	1000	--
Ccc2a (1fvq)	*ESFF1*	72	298	150	1	1000	--
DMAP1 (4iej)	*ESFF1*	75	298	150	1	1000	--
ubiquitin (1ubq)	*ESFF1*	76	298	150	1	1000	--
FKBP12 (2ppn)	*ESFF1*	107	298	150	1	1000	--
LUSH (1ooi)	*ESFF1*	124	298	150	1	1000	--

RS1	***ff14SB, ff14IDPSFF, ESFF1***	**24**	**298**	**150**	**5**	**700 (300~700)**	**Zweckstetter et al. [5]**
Histatin5	***ff14SB, ff14IDPSFF, ESFF1***	**24**	**303**	**0**	**5**	**200 (50~200)**	**Raj et al. [6]**
C-Myb	***ff14SB, ff14IDPSFF, ESFF1***	**25**	**298**	**50**	**5**	**500 (300~500)**	**Wright et al. [7]**
RevARM	***ff14SB, ff14IDPSFF, ESFF1***	**26**	**283**	**150**	**5**	**200 (50~200)**	**18851 [e]**
MevN	***ff14SB, ff14IDPSFF, ESFF1***	**32**	**293**	**100**	**5**	**200 (50~200)**	**6566 [e]**
rIAPP	***ff14SB, ff14IDPSFF, ESFF1***	**35**	**278**	**150**	**5**	**200 (150~200)**	**7311 [e]**
ab40	***ff14SB, ff14IDPSFF, ESFF1***	**40**	**277**	**20**	**5**	**200 (50~200)**	**17796 [e] & Bax et al. [8]**
ab42	***ff14SB, ESFF1***	**42**	**278**	**20**	**5**	**1000 (200~1000)**	**25218 [e] & Bax et al.**
drkN SH3	***ff14SB, ff14IDPSFF, ESFF1***	**59**	**278**	**50**	**5**	**200 (50~200)**	**25501[e] & Marsh et al. [9]**
KID	***ff14SB, ff14IDPSFF, ESFF1***	**61**	**288**	**50**	**5**	**200 (50~200)**	**6784 [e]**
ACTR	***ff14SB, ESFF1***	**71**	**304.15**	**50**	**5×2 [f]**	**500 (50~500)**	**15397 [e]**
IA3	***ff14SB, ff14IDPSFF, ESFF1***	**76**	**293**	**150**	**5**	**200 (50~200)**	**6078 [e]**
p53N	***ff14SB, ff14IDPSFF, ESFF1***	**93**	**293**	**175**	**5**	**200 (50~200)**	**17760 [e]**
tauF4	***ff14SB, ff14IDPSFF, ESFF1***	**124**	**293**	**25**	**5**	**200 (50~200)**	**17945 [e]**
α-synuclein	***ff14SB, ff14IDPSFF, ESFF1***	**140**	**285.5**	**150**	**5**	**200(50~200)**	**6968 [e]**
CBP	***ff14SB, ESFF1***	**59**	**304.15**	**50**	**3**	**500 (50~500)**	**15398 [e]**
ACTR-CBP [g]	***ff14SB, ESFF1***	**71 + 59**	**304.15**	**60**	**3**	**500(50~500)**	**5228 [e]**
p53TAD-CBP [h]	***ff14SB, ESFF1***	**49 + 59**	**298**	**50**	**5**	**500(50~50)**	**17073 [e]**
CLN025	***ESFF1***	**10**	**275~405**	**0**	**14 replicas**	**250 (50~250)**	**Honda et al. [10]**

Trpzip-2	***ESFF1***	**12**	**280~430**	**0**	**16 replicas**	**500 (50~500)**	**Starovasnik et al.** [11]
GB1 hairpin	***ESFF1***	**16**	**275~425**	**0**	**16 replicas**	**500 (250~500)**	**Eaton et al.** [12]
TC5b	***ESFF1***	**20**	**275~410**	**0**	**28 replicas**	**500 (50~500)**	**Andersen et al.** [13]
WW GTT	***ESFF1***	**35**	**280~470**	**0**	**20 replicas**	**1200 (500~1200)**	**Shaw et al.** [14]
villin	***ESFF1***	**36**	**274~426**	**0**	**20 replicas**	**1200 (500~1200)**	**Hofrichter et al.** [15]

[a] X = A, C, D, E, F, H, I, K, L, M, N, Q, R, S, T, V, W and Y. [b] X = A, E, F, K, L, M, S and V. [c] The temperature of 16 trajectories are 275K, 280K, 285K, 290K, 295K, 300K, 305K, 310K, 315K, 320K, 325K, 330K, 335K, 340K, 345K and 350K, respectively. [d] X = D, E, G, H, I, K, L, N, P, Q, T, V, W and Y. [e] Entry ID of BMRB database. [f] One group of 5 trajectories for ff14SB and ESFF1 were simulated from fully folded initial state, while other 5 trajectories were simulated from fully disordered initial state. [g] Complex of ACTR and CBP, where ACTR was reported as a disorder protein, while CBP is a structured protein. [h] Complex of p53TAD and CBP, where p53TAD is a disordered protein.

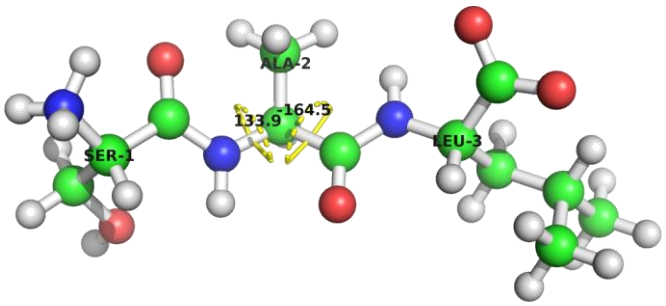

Figure S4. Local sequence environment for ALA in a sample sequence of SER-ALA-LEU.

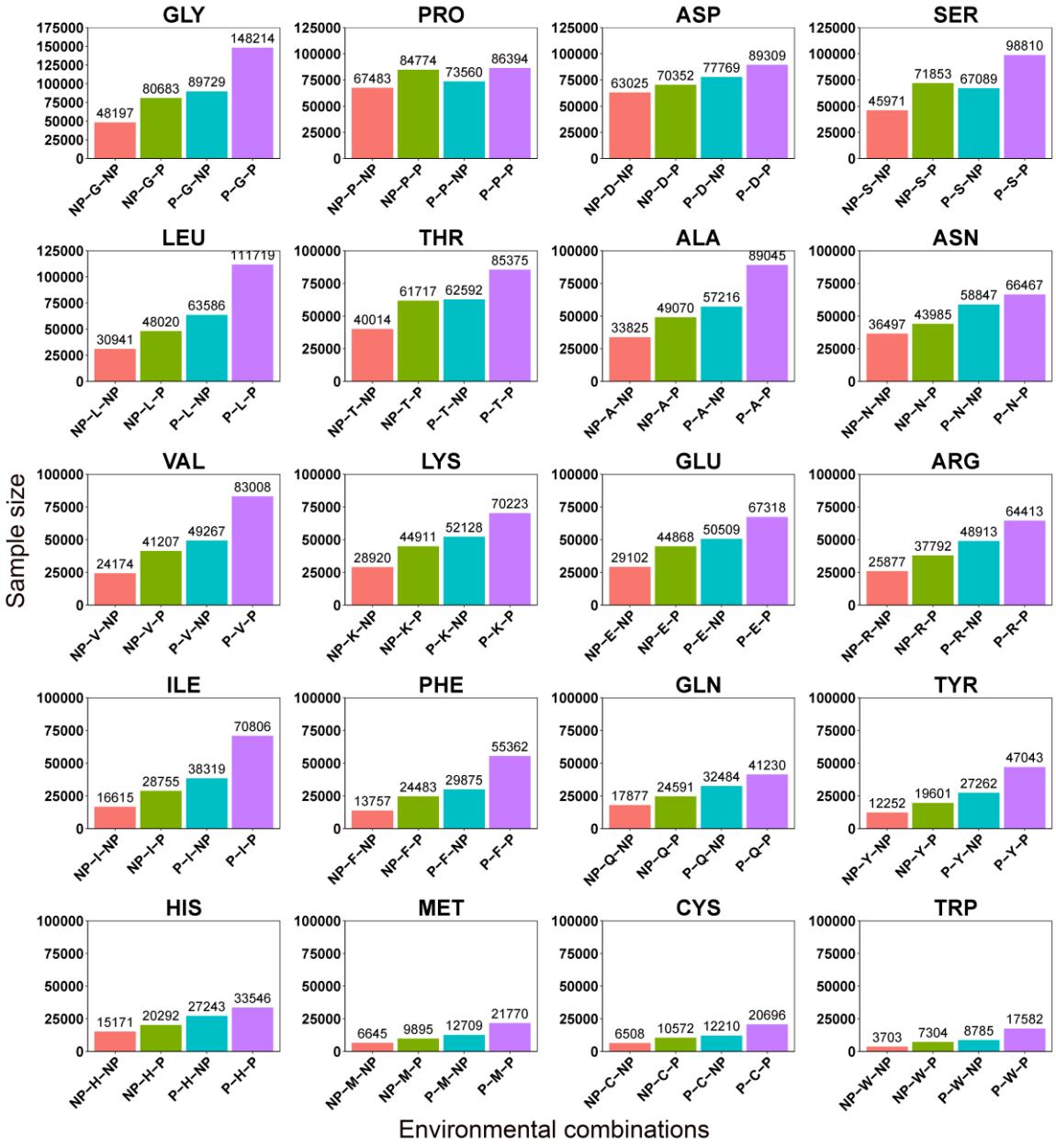

Figure S5. Number of phi/psi samples of all possible environmental combinations of 20 amino acids.

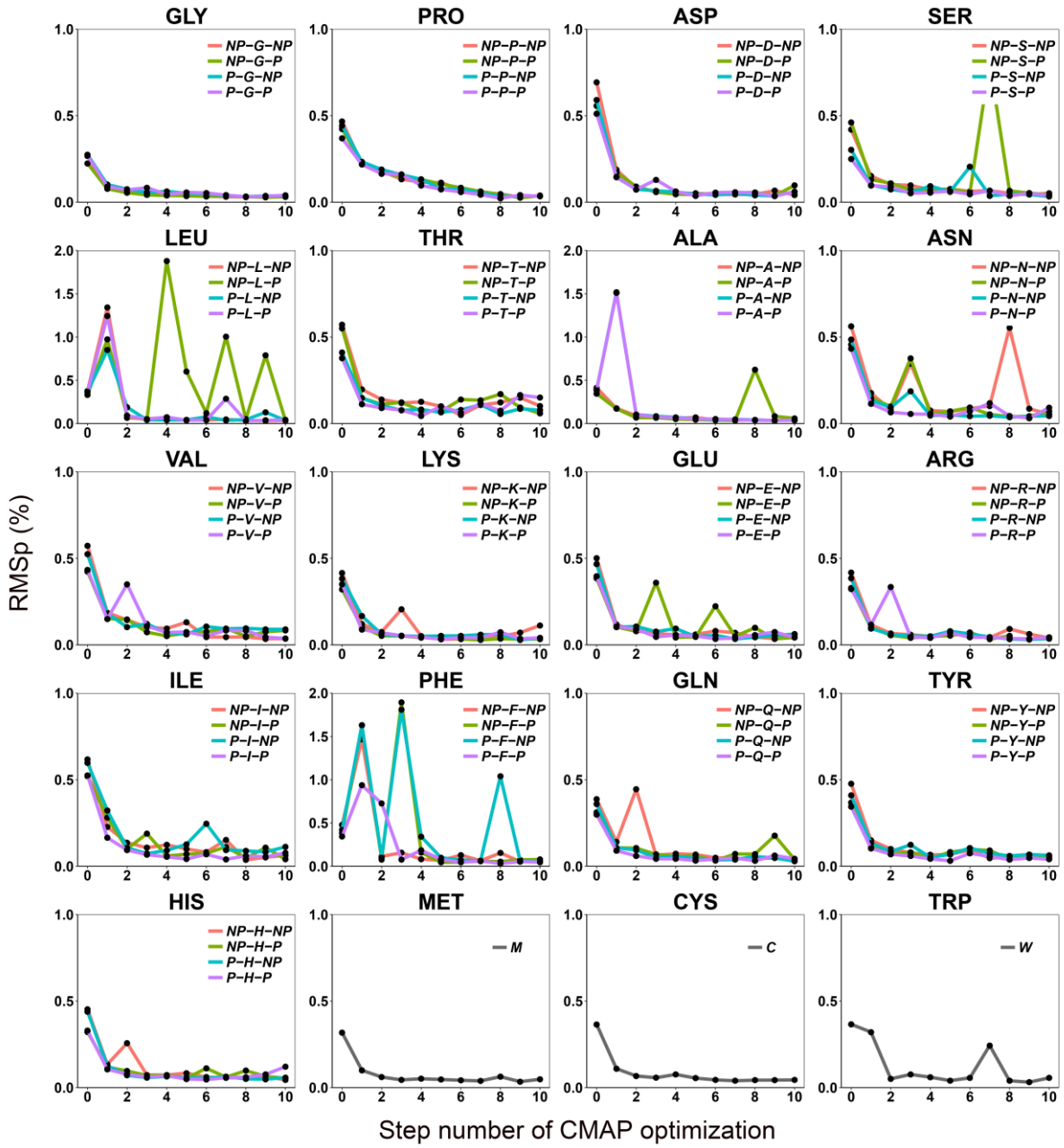

Figure S6. RMSp of CMAP optimization versus optimization iterations for 71 environmental combinations. For MET, CYS, and TRP, all 4 environmental combinations were combined due to insufficient sampling.

Table S2. RMSD's between computed and measured NMR observables for short peptides.

System	RMSD of $\Delta\delta C_\alpha$ [ppm]			RMSD of $^3J(H_N,H_\alpha)$ [Hz]		
	ff14SB	*ff14IDPSFF*	*ESFF1*	*ff14SB*	*ff14IDPSFF*	*ESFF1*
GLY3	0.266	0.231	0.221	0.448	0.090	0.076
VAL3	0.715	0.796	0.789	2.057	0.586	0.355
ALA3	0.132	0.157	0.165	0.367	0.158	0.092
ALA5	0.152	0.166	0.188	0.220	0.166	0.062
ALA7	0.138	0.121	0.109	0.311	0.189	0.038
pepK	0.61	0.14	0.09	0.51	0.35	0.45
pepL	0.68	0.16	0.13	0.60	0.52	0.54
pepQ	0.77	0.18	0.10	1.05	0.61	0.64
pepG	0.45	0.29	0.23	0.66	0.43	0.32
pepT	0.60	0.18	0.20	0.80	0.35	0.39
pepY	0.59	0.13	0.10	0.81	0.71	0.79
pepD	0.98	0.3	0.24	0.92	0.43	0.48
pepE	1.09	0.22	0.16	1.14	0.65	0.59
pepH	0.55	0.27	0.22	1.10	0.55	0.61
pepN	0.64	0.24	0.16	0.82	0.47	0.50
pepI	1.21	0.15	0.14	1.26	0.57	0.59
pepP	0.89	0.17	0.13	0.78	0.70	0.53
pepV	0.92	0.19	0.22	1.19	0.58	0.59
pepW	0.46	0.23	0.14	0.65	0.49	0.48
HEWL19	1.11	0.85	0.80	--	--	--

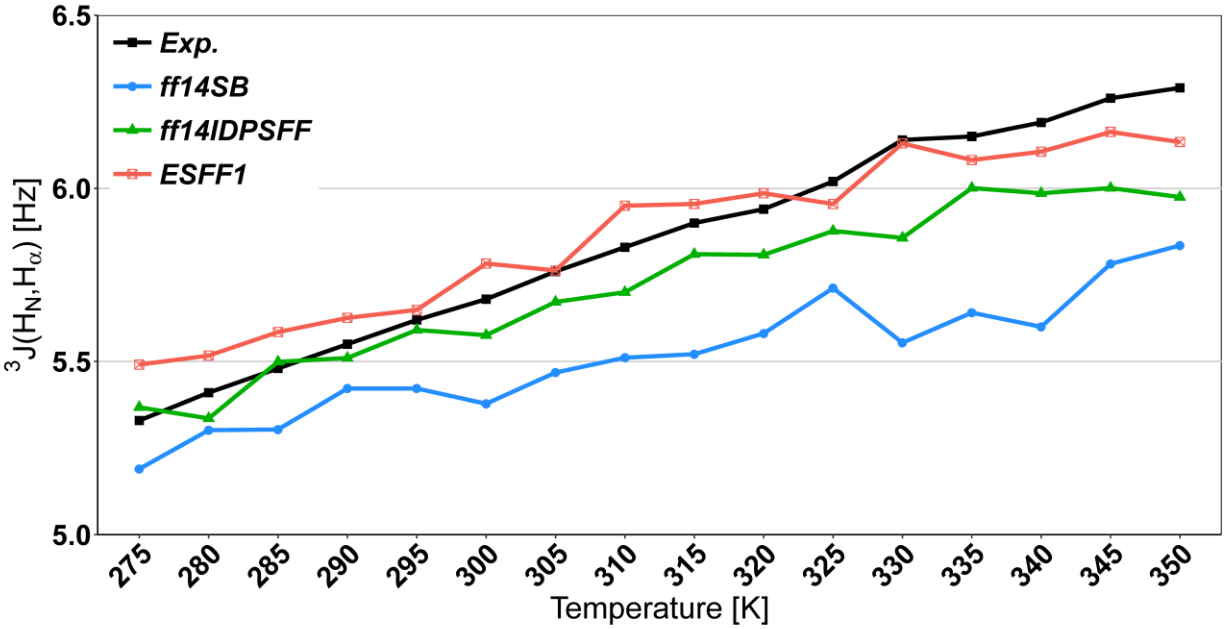

Figure S7. Temperature dependence of $3J(H_N,H_\alpha)$ for the central Alanine in ALA3 in ff14SB, ff14IDPSFF, and ESFF1 simulations.

Table S3. RMSD's between computed and measured $^3J(H_N,H_\alpha)$, $^3J(H_N,C')$ and $^3J(H_N,C_\beta)$ for central residue 'X' in GXG peptides.

System	RMSD of $^3J(H_N,H_\alpha)$ [Hz]			RMSD of $^3J(H_N,C')$ [Hz]			RMSD of $^3J(H_N,C_\beta)$ [Hz]		
	ff14SB	*ff14IDPSFF*	*ESFF1*	*ff14SB*	*ff14IDPSFF*	*ESFF1*	*ff14SB*	*ff14IDPSFF*	*ESFF1*
GAG	0.343	0.139	0.081	0.061	0.015	0.099	0.01	0.292	0.186
GVG	1.329	0.222	0.022	0.150	0.121	0.131	0.597	0.084	0.188
GFG	1.333	0.185	0.168	0.139	0.124	0.07	0.440	0.083	0.052
GSG	0.722	0.302	0.245	0.473	0.264	0.246	0.166	0.114	0.109
GEG	0.866	0.091	0.093	0.035	0.027	0.033	0.676	0.367	0.314
GLG	0.695	0.194	0.261	0.063	0.058	0.114	0.623	0.280	0.310
GKG	0.727	0.446	0.498	--	--	--	--	--	--
GMG	0.988	0.028	0.003	--	--	--	--	--	--

- **Convergence of MD simulations**

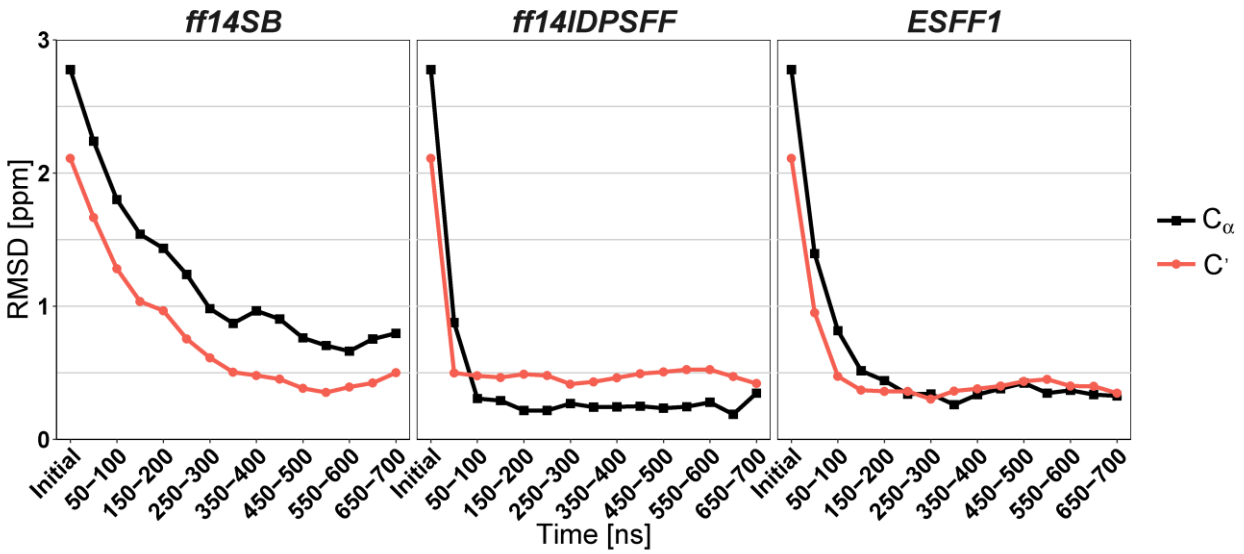

Figure S8. RMSD's between simulated and measured chemical shifts over simulation time (0-50, 50-100, 100-150, 150-200 ns, etc) for RS1.

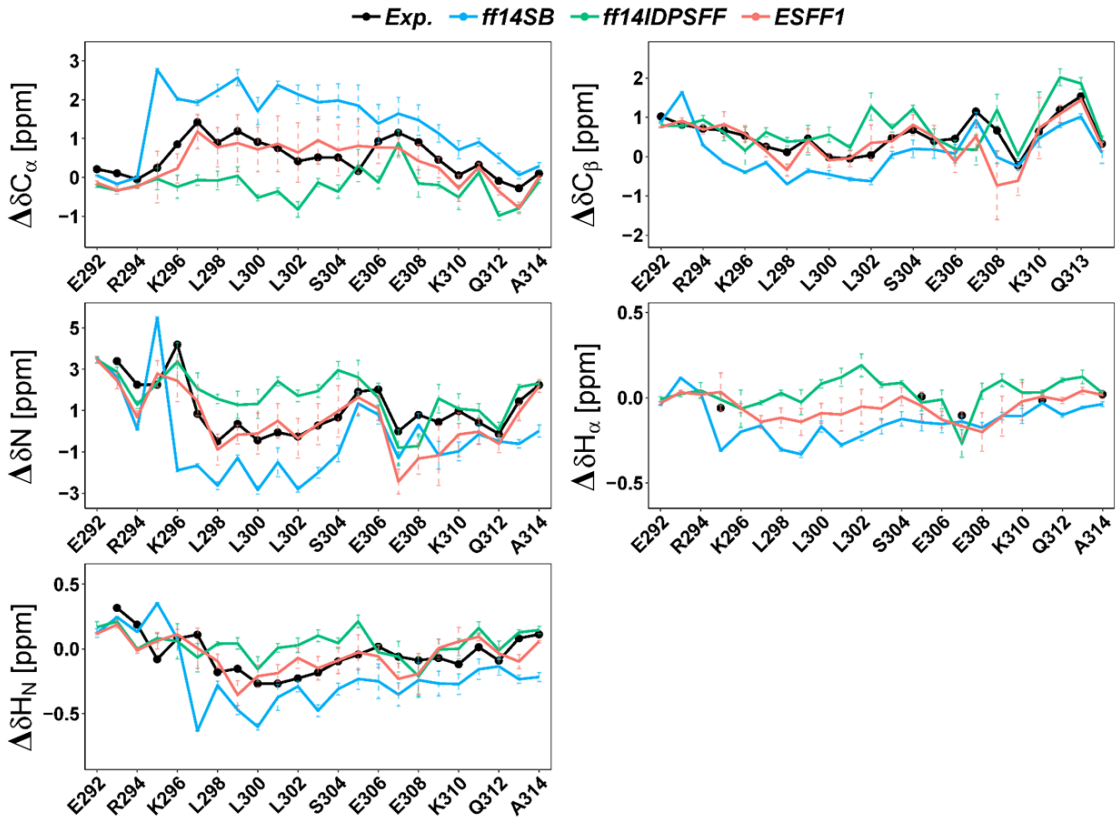

Figure S9. Secondary chemical shifts of c-Myb in *ff14SB*, *ff14IDPSFF*, and *ESFF1* simulations and NMR measurement.

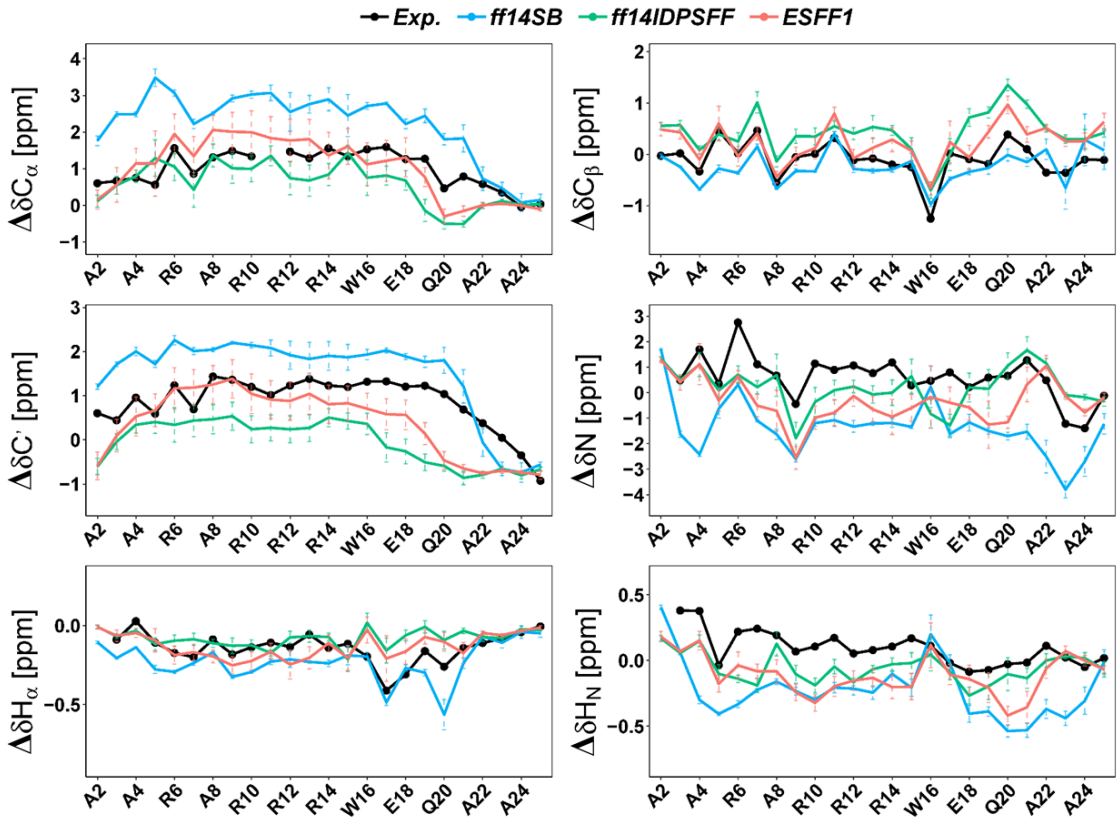

Figure S10. Secondary chemical shifts of RevARM in *ff14SB*, *ff14IDPSFF*, and *ESFF1* simulations and NMR measurement.

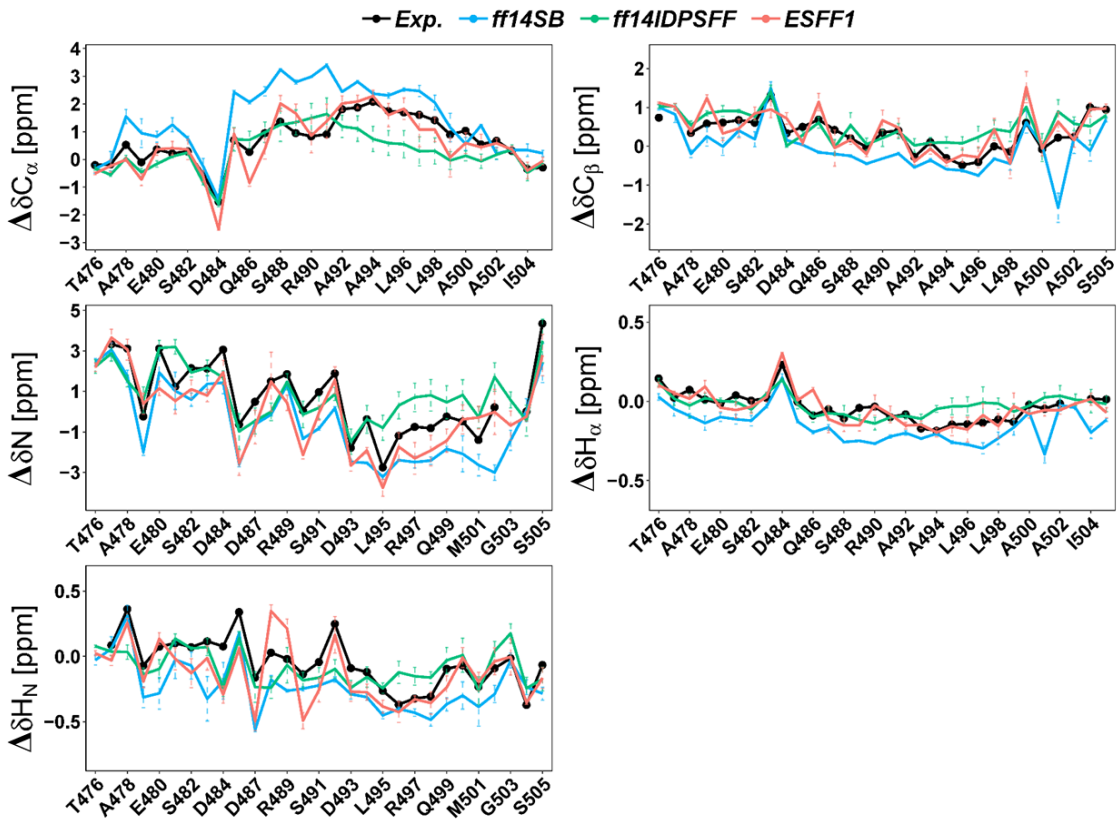

Figure S11. Secondary chemical shift of MevN in *ff14SB*, *ff14IDPSFF*, and *ESFF1* simulations and NMR measurement.

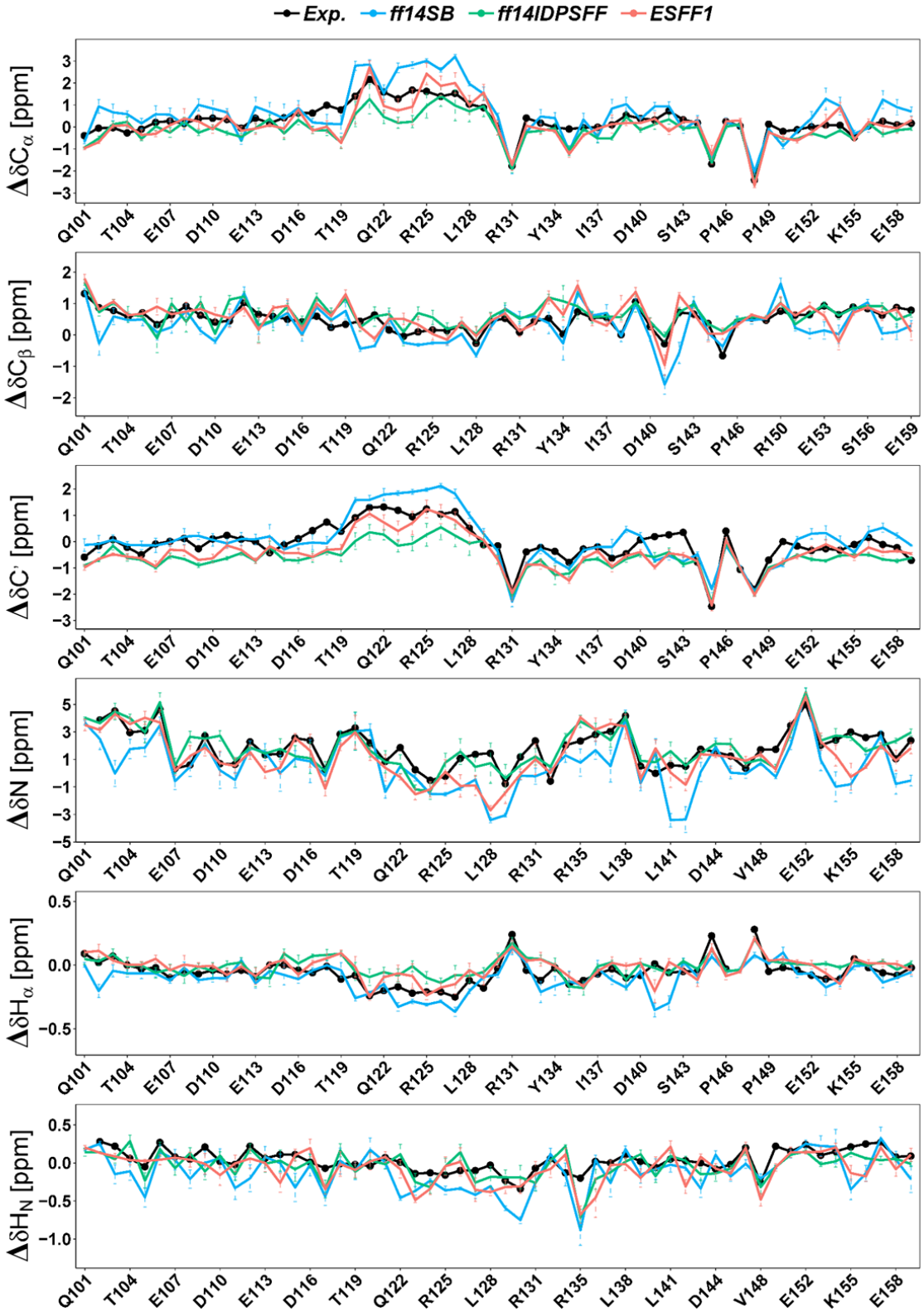

Figure S12. Secondary chemical shifts of KID in *ff14SB*, *ff14IDPSFF*, and *ESFF1* simulations and NMR measurement.

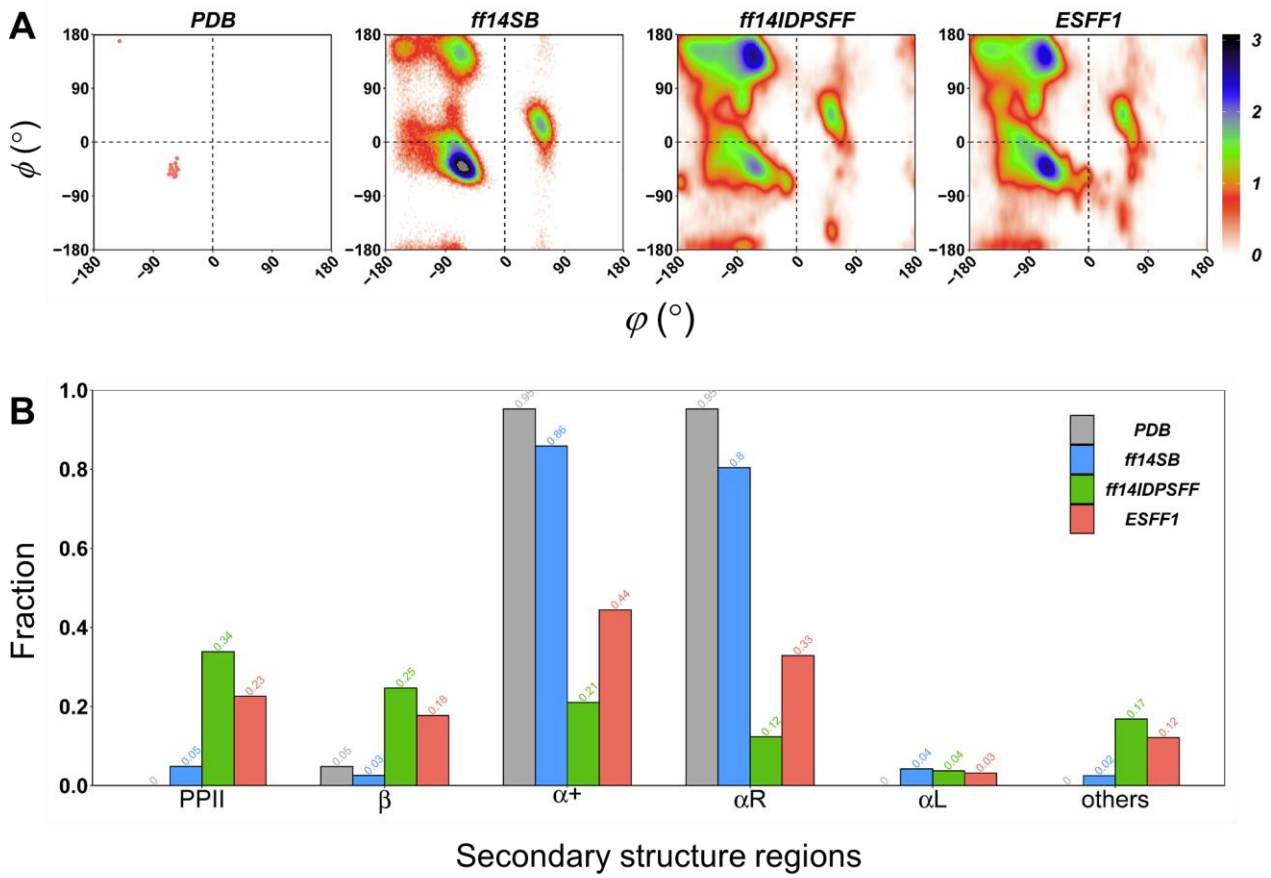

Figure S13. Main chain torsional distributions in MD simulations of RevARM. (A) Ramachandran plots of all non-Pro, non-Gly residues in PDB structures and in simulations with *ff14SB*, *ff14IDPSFF*, and *ESFF1* force fields. (B) Fractions of secondary structure regions in *ff14SB*, *ff14IDPSFF*, and *ESFF1* simulations.

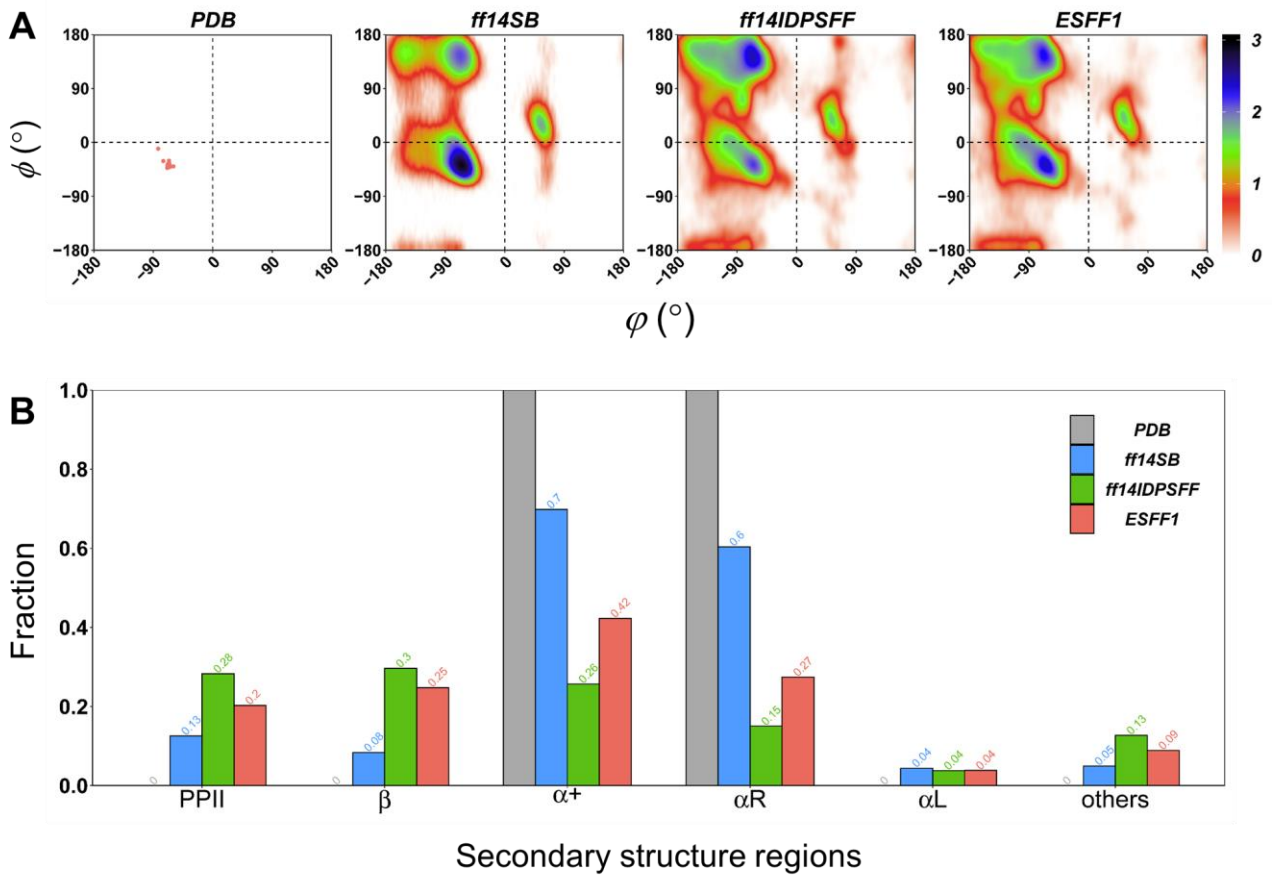

Figure S14. Main chain torsional distributions in MD simulations of MevN. (A) Ramachandran plots of all non-Pro, non-Gly residues in PDB structures and in simulations with *ff14SB*, *ff14IDPSFF*, and *ESFF1* force fields. (B) Fractions of secondary structure regions in *ff14SB*, *ff14IDPSFF*, and *ESFF1* simulations.

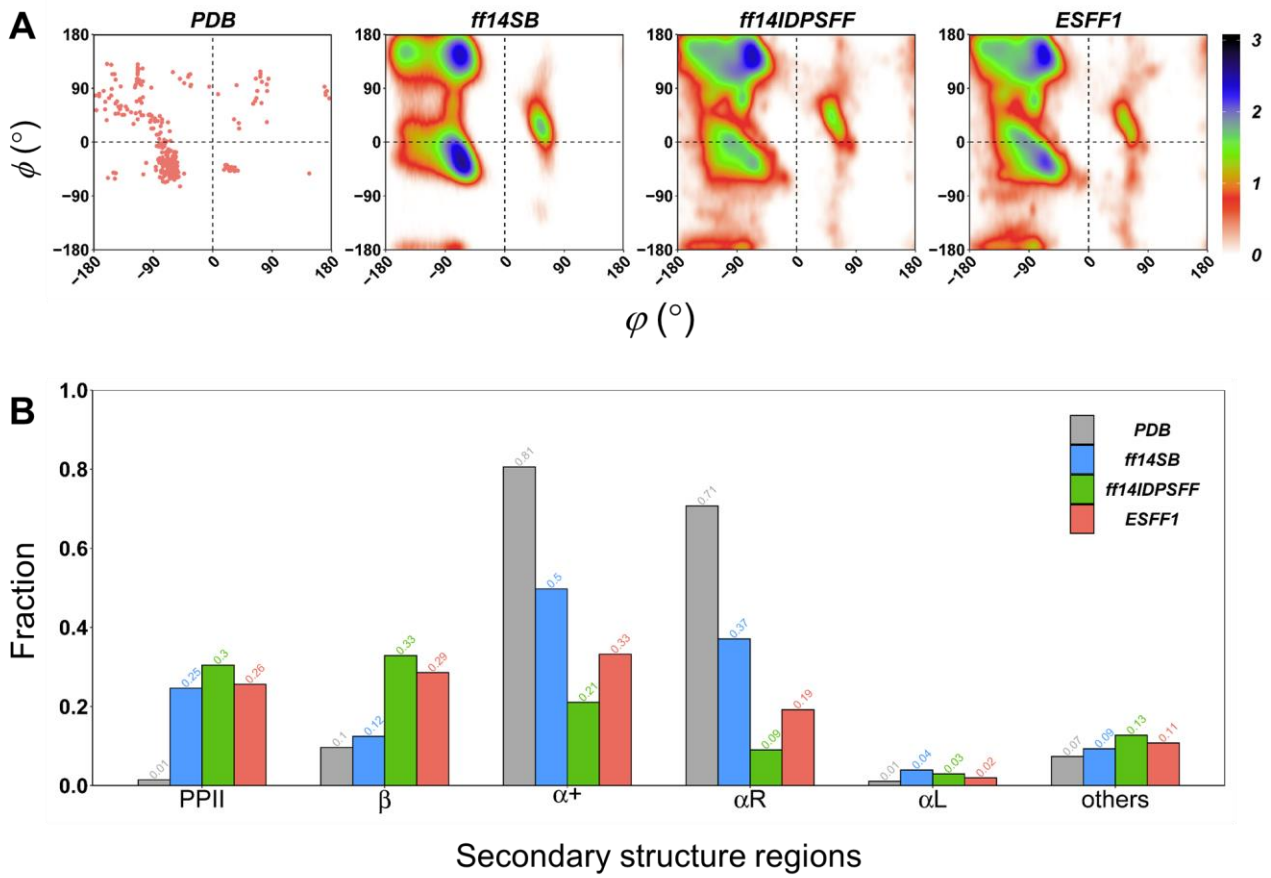

Figure S15. Main chain torsional distributions in MD simulations of KID. (A) Ramachandran plots of all non-Pro, non-Gly residues in PDB structures and in simulations with *ff14SB*, *ff14IDPSFF*, and *ESFF1* force fields. (B) Fractions of secondary structure regions in *ff14SB*, *ff14IDPSFF*, and *ESFF1* simulations.

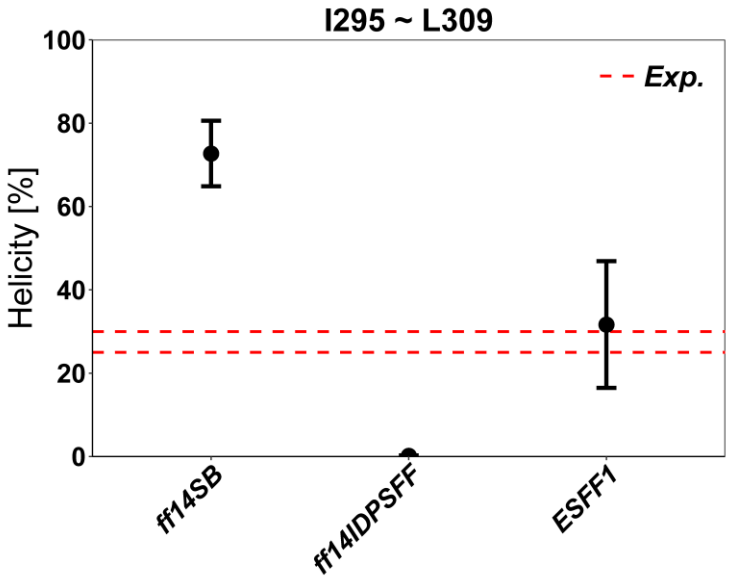

Figure S16. Helicities for segment I295-l309 in c-Myb from *ff14SB*, *ff14IDPSFF* and *ESFF1* simulations. NMR experiment shows that segment I295–L309 of c-Myb exists partially in the helical conformation with around 25–30% helical content[16]. The helicity predicted from *ff14SB* simulations is 72.72% ± 7.85%, 0.19% ± 0.10% from *ff14IDPSFF* simulations and 31.68% ± 15.22% for *ESFF1* simulations.

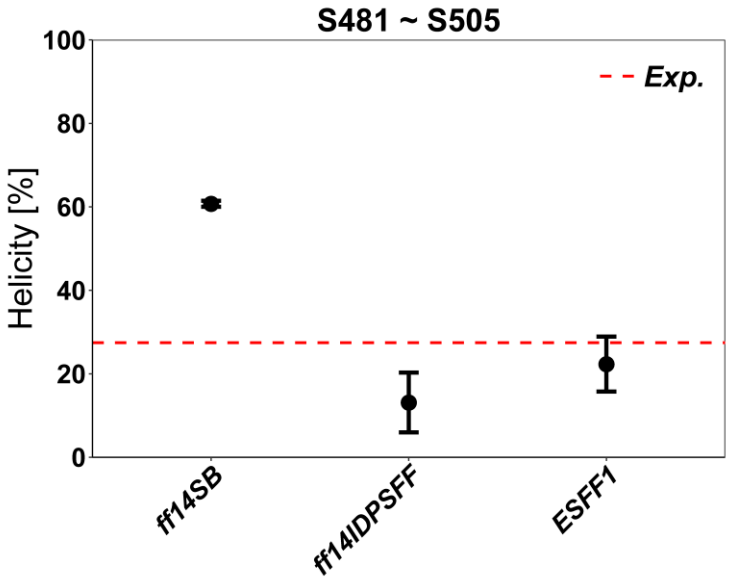

Figure S17. Helicities for segment S481-S505 in MevN from *ff14SB*, *ff14IDPSFF* and *ESFF1* simulations. As reported in Blackledge's experiment[17], the helicity of segment S481-S505 is around 27.44%, The helicity predicted from *ff14SB* simulations is 60.74% ± 0.72%, 13.13% ± 7.15% from *ff14IDPSFF* simulations and 22.32% ± 6.58% for *ESFF1* simulations.

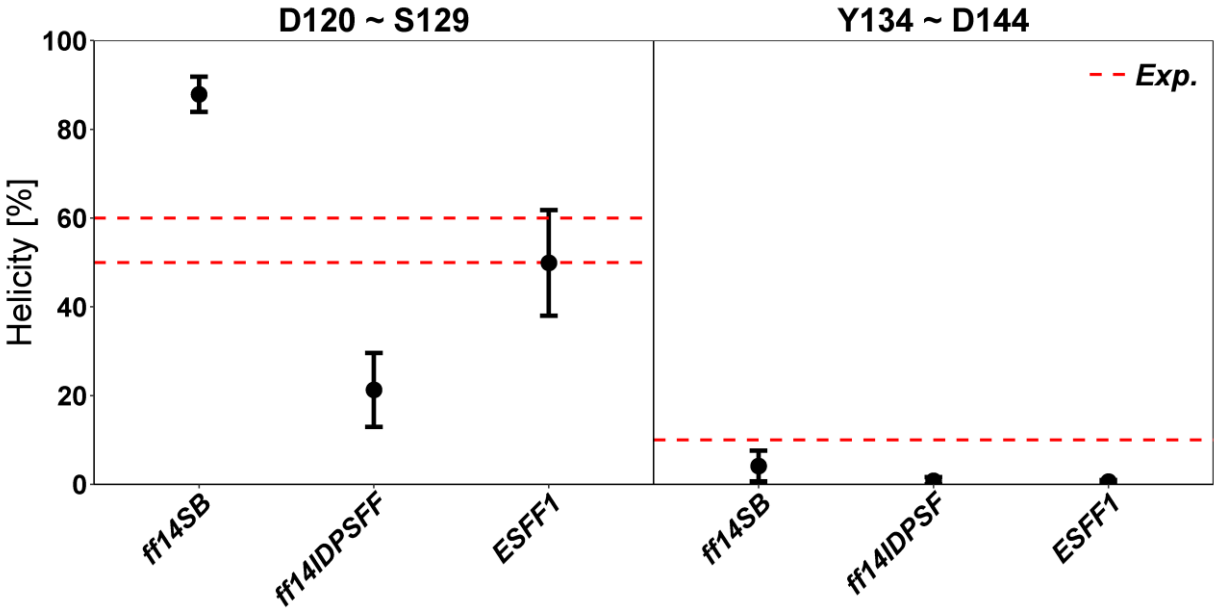

Figure S18. Helicities of segments D120-S129 and Y134-D144 in KID from *ff14SB*, *ff14IDPSFF* and *ESFF1* simulations. In the study of Radhakrishnan and co-workers the helicities of αA (D120−S129) and αB (Y134−D144) of KID are between 50% and 60% and 10%, respectively[18]. The helicities predicted from *ff14SB* simulations are 87.89% ± 3.98% for αA and 4.14% ± 3.44% for αB, 21.30% ± 8.33% for αA and 0.82% ± 0.81% for αB from *ff14IDPSFF* simulations. In the *ESFF1* simulations, the helicity of αA is 49.92% ± 11.91%, and that of αB is 0.63% ± 0.34%.

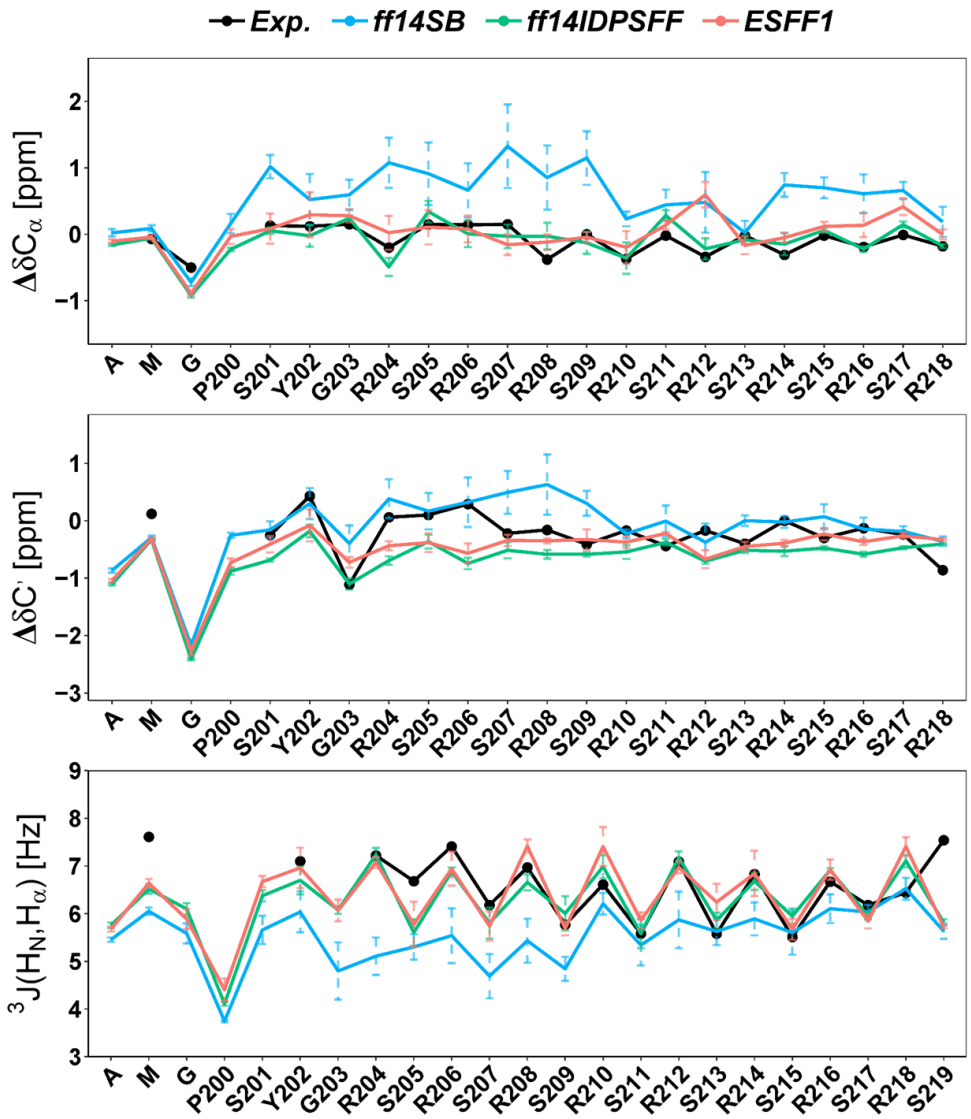

Figure S19. Secondary chemical shifts and $^{3}J(H_N,H_\alpha)$ of RS1 in *ff14SB*, *ff14IDPSFF*, and *ESFF1* simulations and NMR measurement.

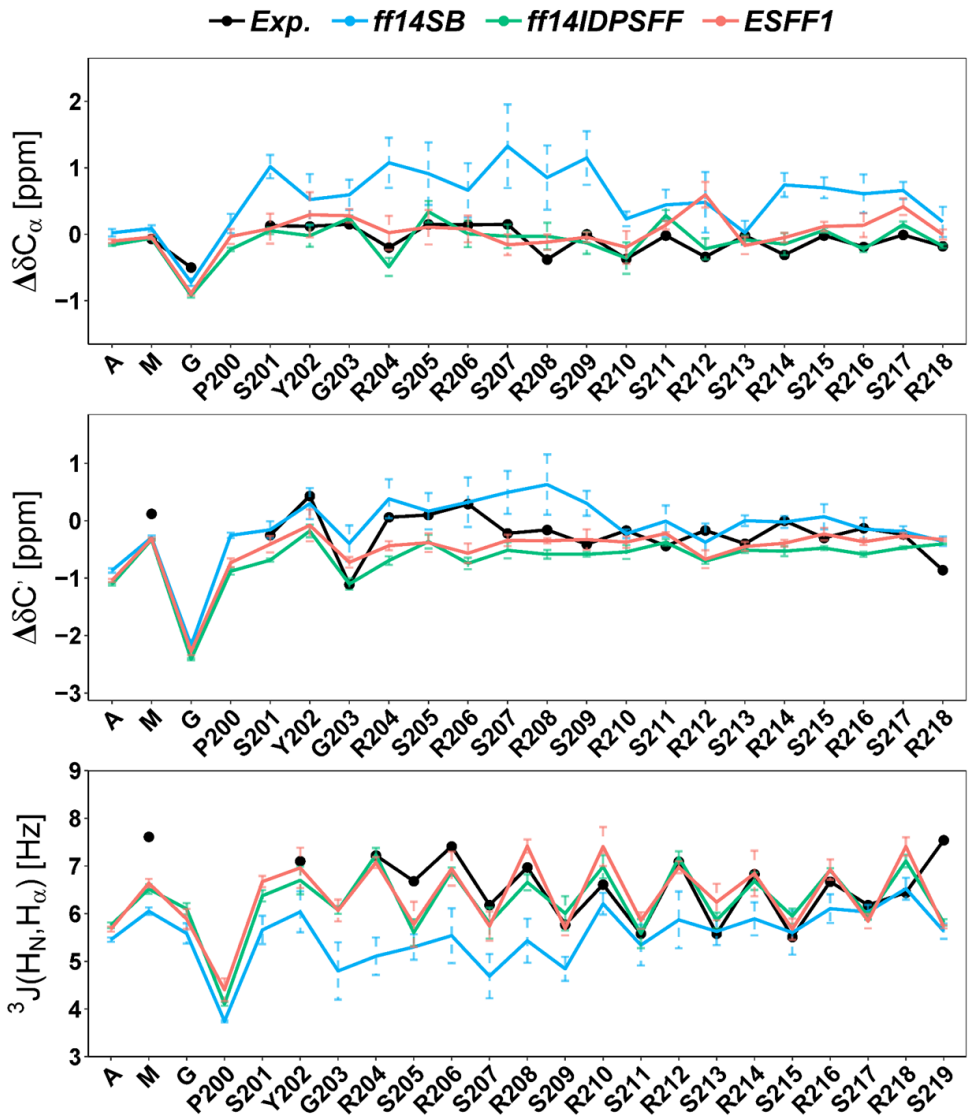

Figure S20. Secondary chemical shifts and $^{3}J(H_N,H_\alpha)$ of RS1 the *ff14SB* and *ESFF1* simulations and NMR measurement. Simulations in both TIP3P and TIP4P-D solvent models were tested.

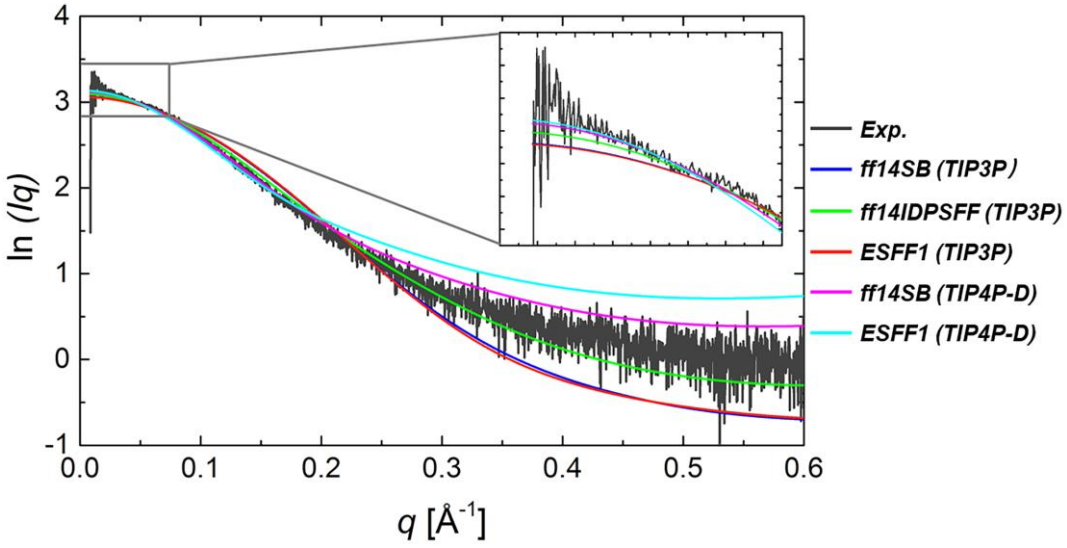

Figure S21. SAXS of RS1 from MD simulations compared with experimental data.

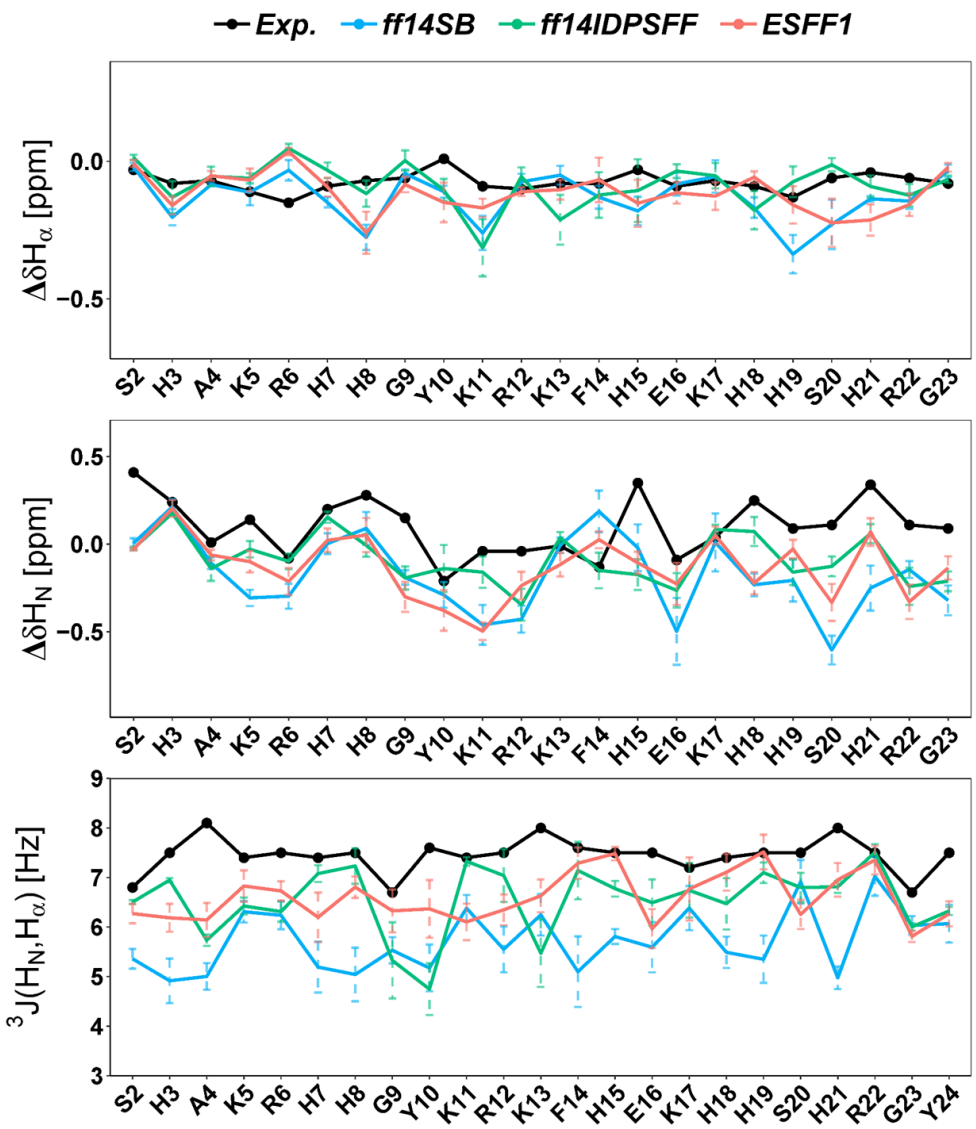

Figure S22. Secondary chemical shifts and $^{3}J(H_N,H_\alpha)$ of Histatin5 in *ff14SB*, *ff14IDPSFF*, and *ESFF1* simulations and NMR measurement.

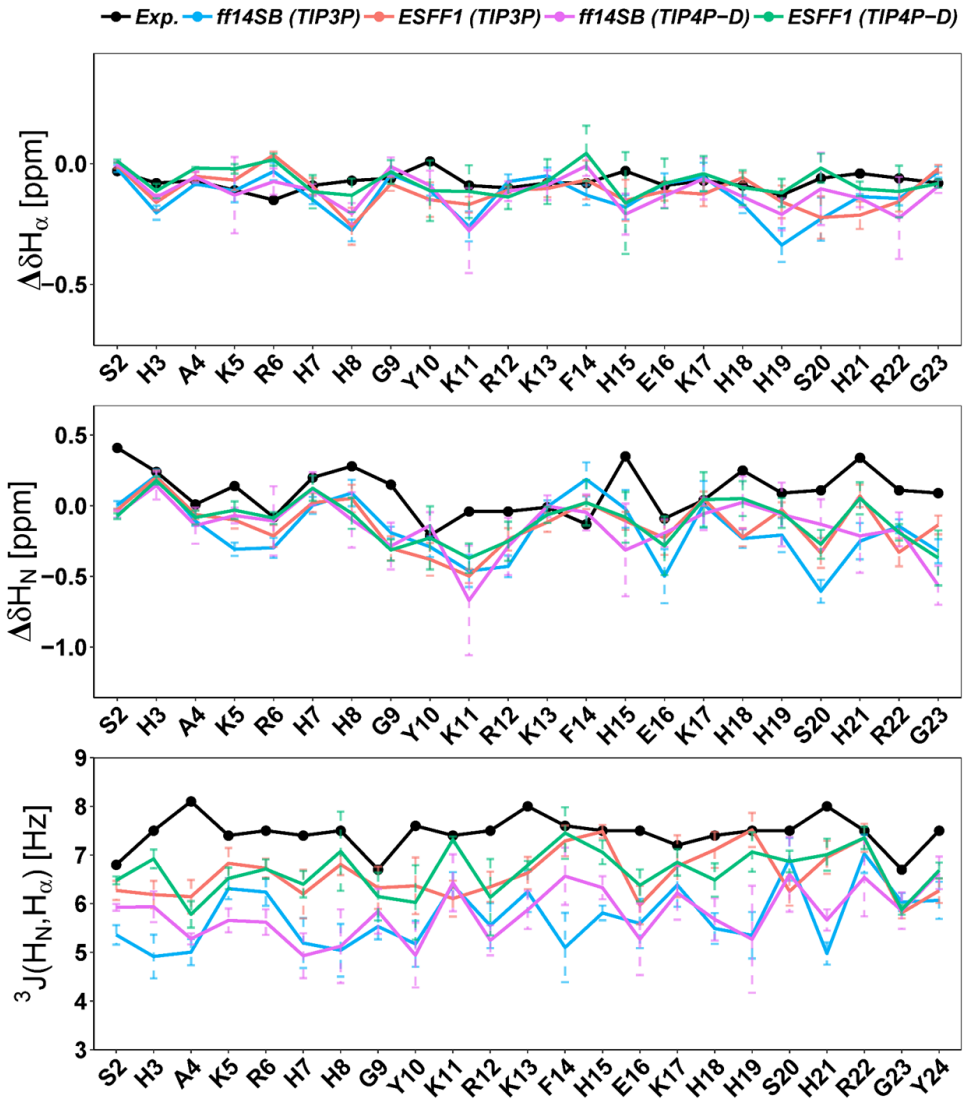

Figure S23. Secondary chemical shifts and $^{3}J(H_N,H_\alpha)$ of Histatin5 from the *ff14SB* and *ESFF1* simulations and NMR measurement. Simulations in both TIP3P and TIP4P-D solvent models were tested.

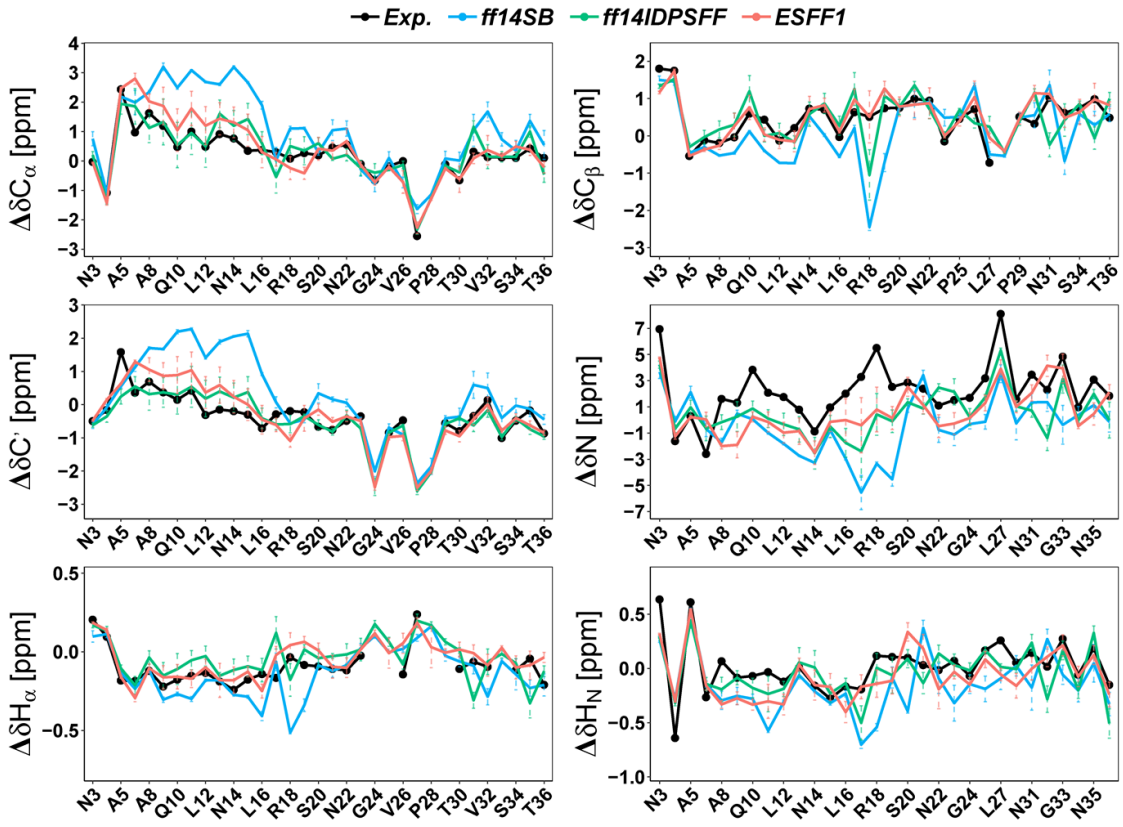

Figure S24. Secondary chemical shifts of rIAPP in *ff14SB*, *ff14IDPSFF*, and *ESFF1* simulations and NMR measurement.

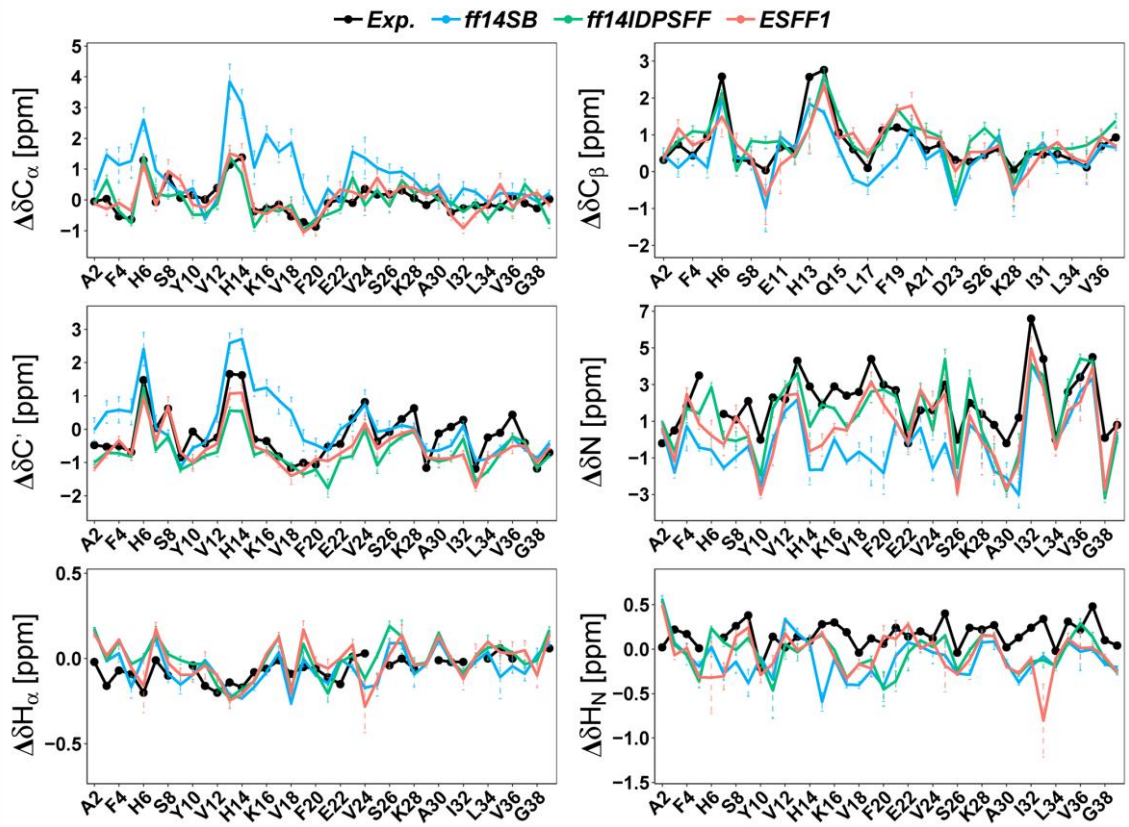

Figure S25. Secondary chemical shifts of ab40 in *ff14SB*, *ff14IDPSFF*, and *ESFF1* simulations and NMR measurement.

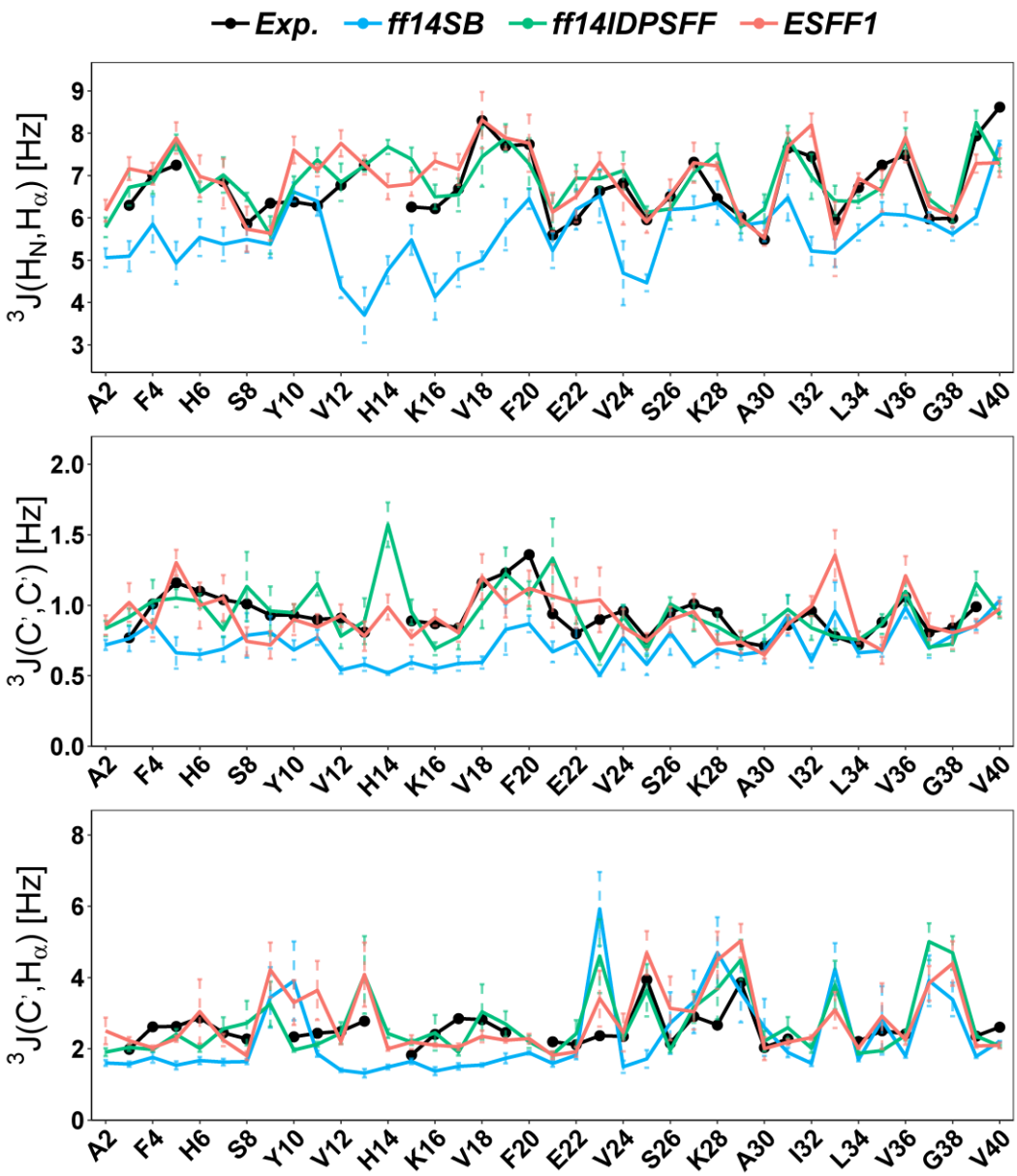

Figure S26. J-coupling constants of ab40 from *ff14SB*, *ff14IDPSFF*, and *ESFF1* simulations and NMR measurement.

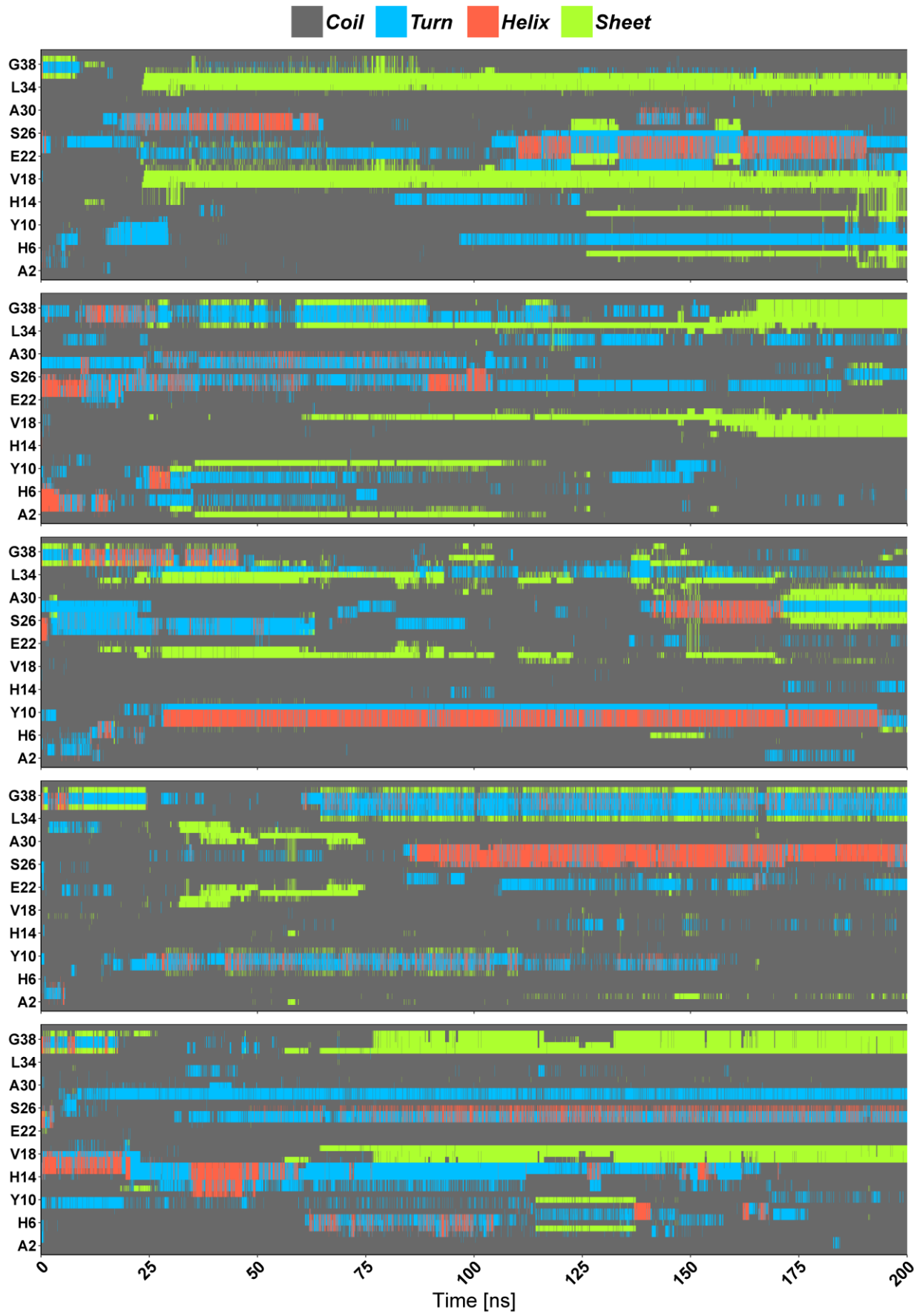

Figure S27. Secondary structure evolution of ab40 in *ESFF1*simulations (5 trajectories). Takahiro et al showed there was a dynamic equilibrium between a random coil and a hairpin-like turn at around D23–A30 based on their NMR measurements[19]. This equilibrium was also detected in trajectories (except the 4th trajectory above) of *ESFF1*simulations.

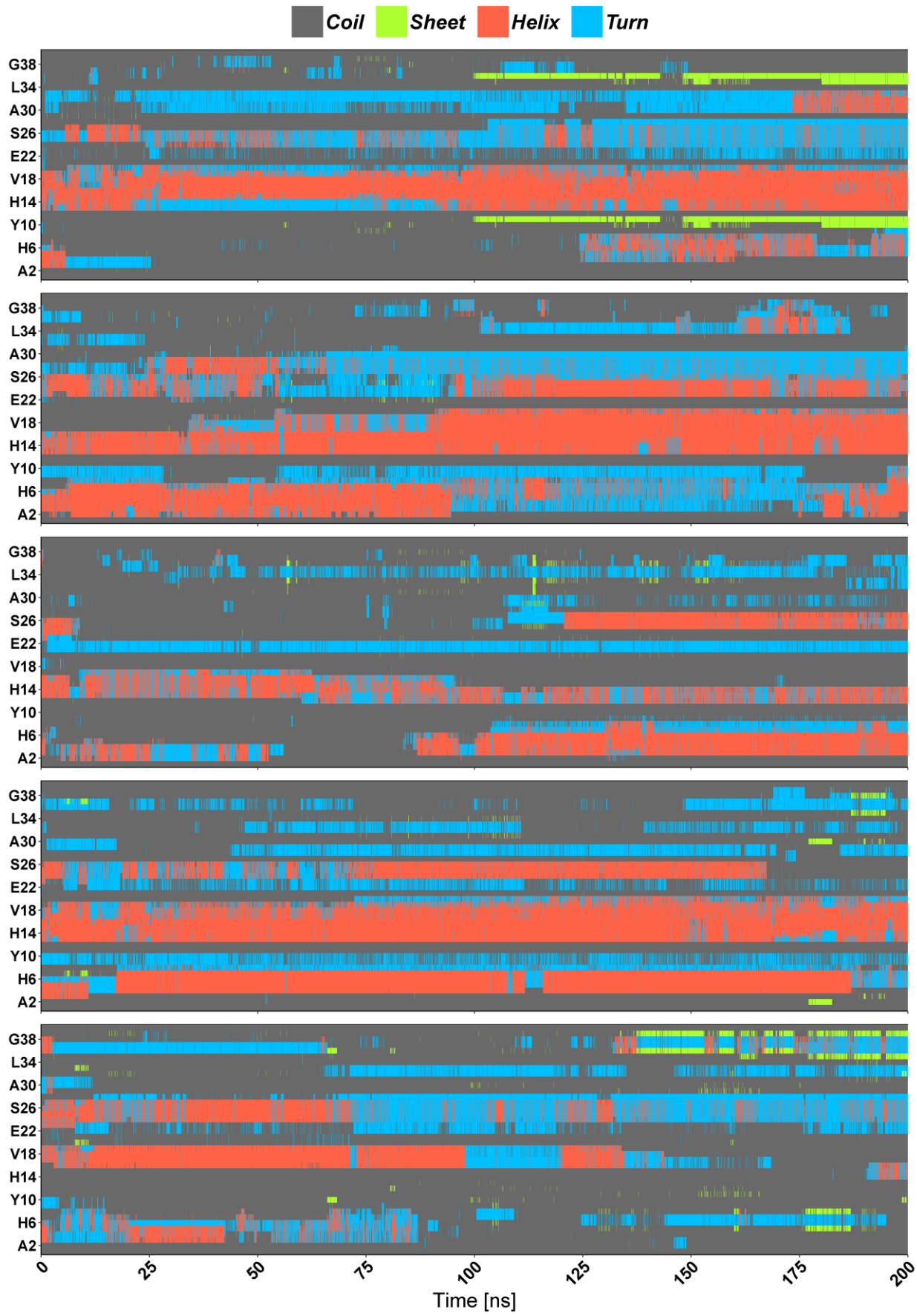

Figure S28. Secondary structure evolution of ab40 in *ff14SB* simulations (5 trajectories). The dynamic equilibrium between a random coil and a hairpin-like turn at around D23–A30 was not reproduced in *ff14SB* simulations.

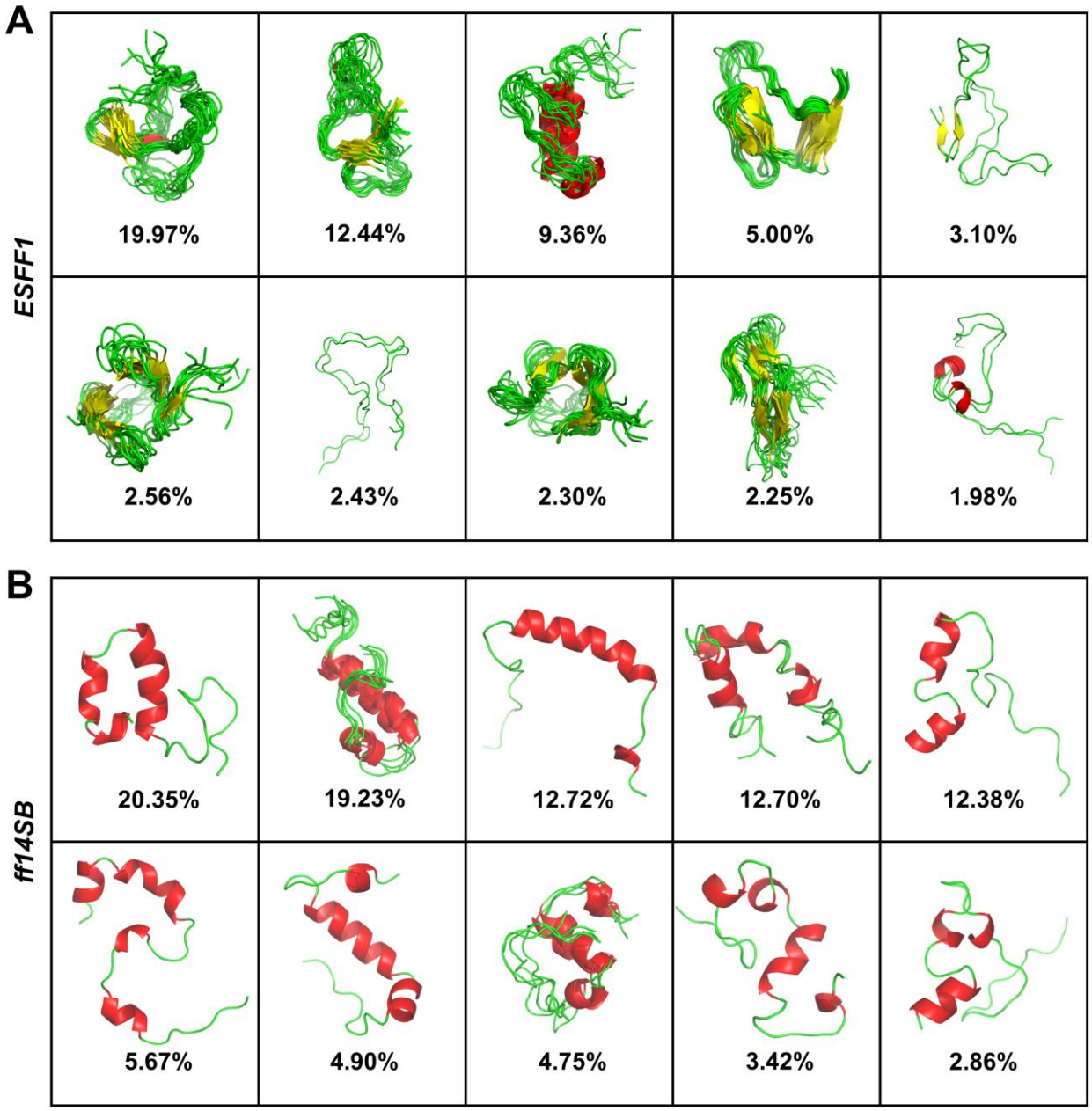

Figure S29. Conformer clusters of ab42 in 5 trajectories of 1000 ns each. (A) Dominated conformers and corresponding percentage of ab42 in *ESFF1* simulations. (B) Dominated conformers and corresponding percentage of ab42 in *ff14SB* simulations. The conformer distributions of ab42 indicate that conformers in *ff14SB* simulations tend to adopt compact molten globule-like structures. While conformers in *ESFF1* simulations sample a wide range of structures of β-sheet, random coil and a few parts of α-helix. As shown in previous experimental CD spectra taken immediately after the dissolution of ab42, ab42 has 3%~9% α-helix and 12%~25% β-sheet[20]. In *ESFF1* simulations 6.77% α-helix and 18.68% β-sheet were detected, while in *ff14SB* simulations 37.97% α-helix and only 1.88% β-sheet were found.

Table S4. Rg and RMSD's of secondary chemical shifts for c-Myb.

	ff14SB/TIP3P	*ff14IDPSFF/TIP3P*	*ESFF1/TIP3P*
Rg*	10.49	11.82	11.16
C_α	1.092	0.847	0.337
C_β	0.540	0.480	0.389
N	2.223	1.264	1.043
H_α	0.135	0.081	0.057
H_N	0.273	0.162	0.117

*No experimental Rg is reported.

Table S5. Rg and RMSD's of secondary chemical shifts for RevARM.

	ff14SB/TIP3P	*ff14IDPSFF/TIP3P*	*ESFF1/TIP3P*
Rg*	10.40	13.42	10.73
C_α	1.335	0.645	0.480
C_β	0.316	0.583	0.417
C'	0.796	1.019	0.682
N	2.238	0.997	1.361
H_α	0.121	0.112	0.095
H_N	0.382	0.195	0.255
$^3J(H_N,H_\alpha)$	1.481	0.742	0.766

*No experimental Rg is reported.

Table S6. Rg and RMSD's of secondary chemical shifts for MevN.

	ff14SB/TIP3P	*ff14IDPSFF/TIP3P*	*ESFF1/TIP3P*
Rg*	10.75	13.46	11.02
C_α	1.082	0.657	0.450
C_β	0.566	0.343	0.338
N	1.510	1.086	1.146
H_α	0.136	0.068	0.060
H_N	0.225	0.162	0.178

*No experimental Rg is reported.

Table S7. Rg and RMSD's of secondary chemical shifts for KID.

	ff14SB/TIP3P	*ff14IDPSFF/TIP3P*	*ESFF1/TIP3P*
Rg*	16.94	16.40	14.94
C_α	0.678	0.561	0.483
C_β	0.491	0.360	0.397
C'	0.500	0.654	0.495
N	1.872	0.822	1.218
H_α	0.100	0.085	0.077
H_N	0.252	0.163	0.196

*No experimental Rg is reported.

Table S8. Rg and RMSD's of secondary chemical shifts and J-coupling for RS1.

	ff14SB/TIP3P	*ff14IDPSFF/TIP3P*	*ESFF1/TIP3P*	*ff14SB/TIP4P-D*	*ESFF1/TIP4P-D*
Rg*	10.17	11.71	9.96	13.92	15.41
C_α	0.775	0.221	0.298	0.295	0.159
C'	0.413	0.407	0.379	0.347	0.420
$^3J(H_N,H_\alpha)$	1.190	0.626	0.667	0.972	0.586

*Experimental Rg for RS1 is 12.62±0.07 Angstrom[21].

Table S9. Rg and RMSD's of secondary chemical shifts and J-coupling constants for Histatin5.

	ff14SB/TIP3P	*ff14IDPSFF/TIP3P*	*ESFF1/TIP3P*	*ff14SB/TIP4P-D*	*ESFF1/TIP4P-D*
Rg*	10.15	10.38	10.51	13.97	14.92
H_α	0.105	0.088	0.096	0.081	0.069
H_N	0.355	0.244	0.290	0.286	0.269
$^3J(H_N,H_\alpha)$	1.838	1.153	0.977	1.741	0.911

*Experimental Rg for Histatin5 is 13.8 Angstrom[22].

Table S10. Rg and RMSD's of secondary chemical shifts for rIAPP.

	ff14SB/TIP3P	*ff14IDPSFF/TIP3P*	*ESFF1/TIP3P*
Rg*	11.25	14.01	11.10
C_α	1.183	0.442	0.509
C_β	0.769	0.560	0.303
C'	1.117	0.384	0.462
N	3.723	2.375	2.304
H_α	0.143	0.116	0.083
H_N	0.299	0.179	0.193

*No experimental Rg is reported.

Table S11. Rg and RMSD's of secondary chemical shifts and J-coupling for ab40.

	ff14SB/TIP3P	*ff14IDPSFF/TIP3P*	*ESFF1/TIP3P*	*ff14SB/TIP4P-D*	*ESFF1/TIP4P-D*
Rg*	11.62	15.34	12.25	17.57	19.22
C_α	1.115	0.409	0.310	0.880	0.418
C_β	0.554	0.480	0.453	0.610	0.386
C'	0.769	0.629	0.506	0.664	0.555
N	2.651	1.444	1.773	2.590	1.455
H_α	0.107	0.114	0.120	0.120	0.115
H_N	0.381	0.298	0.332	0.334	0.280
$^3J(H_N,H_\alpha)$	1.481	0.569	0.577	1.212	0.606
$^3J(C',C')$	0.275	0.141	0.162	0.205	0.109
$^3J(C',H_\alpha)$	1.148	0.625	0.675	1.013	0.553

*Experimental Rg for ab40 is 12.0±1.3 Angstrom[23].

Table S12. Rg and RMSD's of secondary chemical shifts and $^3J(H_N,H_\alpha)$ for ab42

	ff14SB/TIP3P	*ESFF1/TIP3P*
Rg*	11.02	11.27
C_α	1.472	0.371
C_β	0.581	0.489
N	2.923	1.891
H_α	0.184	0.230
H_N	0.298	0.210
$^3J(H_N,H_\alpha)$	1.631	0.606

* No experimental Rg is reported.

Table S13. Rg and RMSD's of secondary chemical shifts for drkN SH3.

	ff14SB/TIP3P	*ff14IDPSFF/TIP3P*	*ESFF1/TIP3P*	*ff14SB/TIP4P-D*	*ESFF1/TIP4P-D*
Rg*	13.22	19.03	14.97	22.55	25.59
C_α	0.887	0.687	0.487	0.754	0.709
C_β	0.672	0.594	0.478	0.663	0.536
C'	0.784	0.943	0.856	0.826	0.998
H_α	0.137	0.120	0.095	0.114	0.103
H_N	0.336	0.206	0.233	0.328	0.249
$^3J(H_N,H_\alpha)$	0.989	1.170	0.999	1.687	0.839

*Experimental Rg for drkN SH3 is 16.7±1.4 Angstrom[24].

Table S14. Rg and RMSD's of secondary chemical shifts for ACTR. The MD simulation for ACTR with PDB initial structure was started from a half folded structure where the folded segment E23-K71 was extracted from PDB 1KBH and the remaining random coil at the N terminus was modeled by I-TASSER[25]. A second set of MD simulations with extended initial structure was started from a fully disordered conformer that obtained from 10 ns NVT high-temperature MD of 500 K.

	PDB initial structure				**Extended initial structure**	
	ff14SB/TIP3P	*ESFF1/TIP3P*	*ff14SB/TIP4P-D*	*ESFF1/TIP4P-D*	*ff14SB/TIP3P*	*ESFF1/TIP3P*
Rg	17.37	17.20	20.98	27.35	15.65	15.60
C_α	1.288	0.719	0.864	0.627	0.743	0.520
C_β	0.575	0.353	0.412	0.321	0.427	0.418
C'	1.090	0.634	0.740	0.625	0.666	0.567
N	1.912	1.420	1.524	1.006	1.850	1.070
H_N	0.208	0.178	0.166	0.159	0.208	0.181

*Experimental Rg for ACTR is 25±1.0 Angstrom[26].

Table S15. Rg and RMSD's of secondary chemical shifts for IA3.

	ff14SB/TIP3P	*ff14IDPSFF/TIP3P*	*ESFF1/TIP3P*
Rg*	16.11	16.37	16.79
C_α	1.433	0.569	0.448
C'	1.104	0.866	0.706
N	3.042	1.659	1.932
H_α	0.205	0.141	0.130
H_N	0.336	0.179	0.190

*No experimental Rg is reported.

Table S16. Rg and RMSD's of secondary chemical shifts for p53N.

	ff14SB/TIP3P	*ff14IDPSFF/TIP3P*	*ESFF1/TIP3P*
Rg*	17.02	19.37	17.89
C_α	1.178	0.601	0.721
C_β	0.903	0.69	0.703
C'	0.676	0.524	0.537
N	2.847	1.650	1.812
H_N	0.332	0.253	0.308

*No experimental Rg is reported.

Table S17. Rg and RMSD's of secondary chemical shifts for tauF4.

	ff14SB/TIP3P	*ff14IDPSFF/TIP3P*	*ESFF1/TIP3P*
Rg*	20.43	20.70	21.41
C_α	1.169	0.750	0.616
C_β	0.651	0.570	0.590
N	2.711	1.481	1.897
H_N	0.333	0.197	0.222

*No experimental Rg is reported.

Table S18. Rg and RMSD's of secondary chemical shifts for α-synuclein.

	ff14SB/TIP3P	*ff14IDPSFF/TIP3P*	*ESFF1/TIP3P*
Rg*	22.95	28.99	27.69
C_α	0.998	0.604	0.620
C_β	0.433	0.341	0.396
C'	0.540	0.675	0.620
N	2.566	1.444	1.819
H_α	0.165	0.112	0.127
H_N	0.292	0.235	0.246
$^3J(H_N,H_\alpha)$	1.384	0.546	0.669
$^3J(C',C')$	0.184	0.194	0.175

*Experimental Rg for α-synuclein is 27 ~ 35 Angstrom[27, 28].

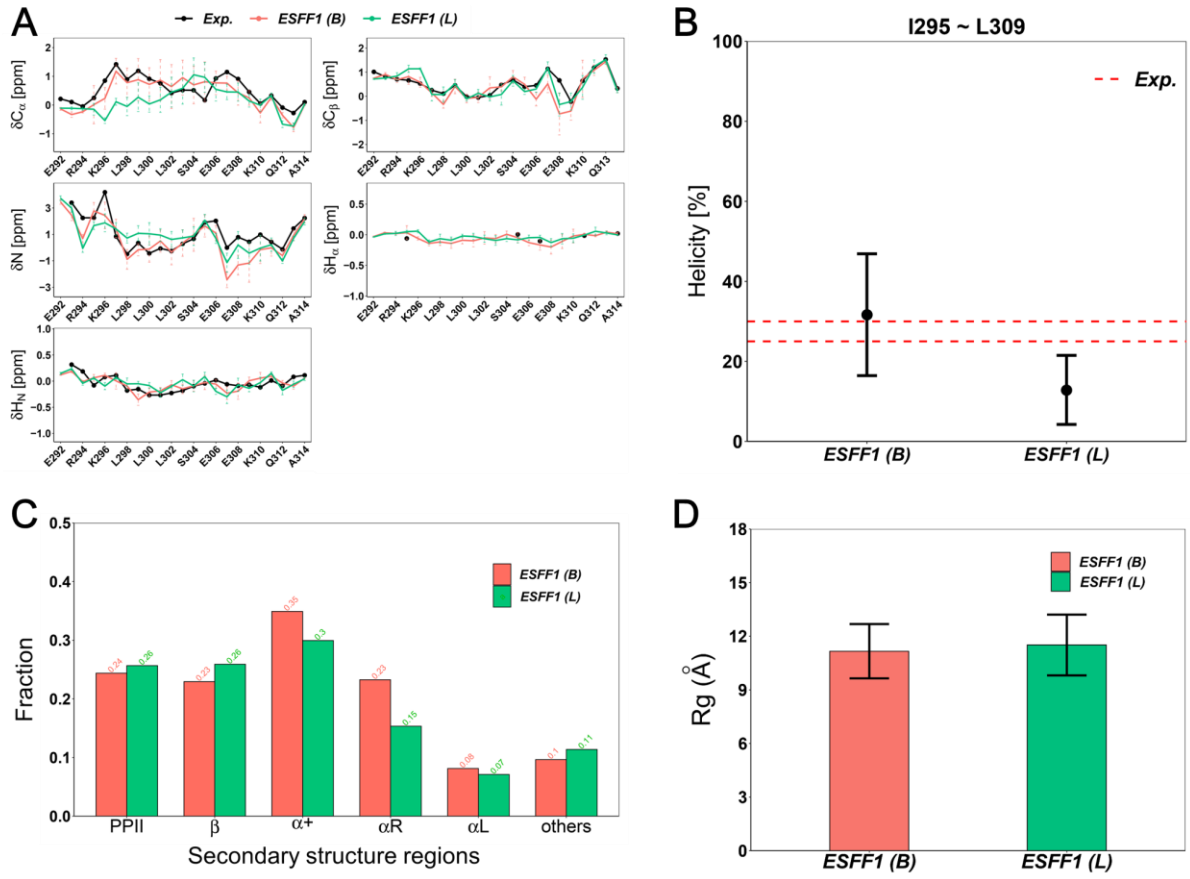

Figure S30. Comparison of the simulate results of c-Myb using *ESFF1* force field with two different thermostats ("B" for Berendsen and "L" for Langevin). (A) Secondary chemical shifts. (B) Helicity of I295 ~ L309 fragment. (C) Fractions of secondary structure regions. (D) Ensemble-averaged Rg. The two simulations are similar with each other except small difference in helicity of I295 ~ K309 and thus result in several lower values in Cα secondary chemical shifts compared with experimental data.

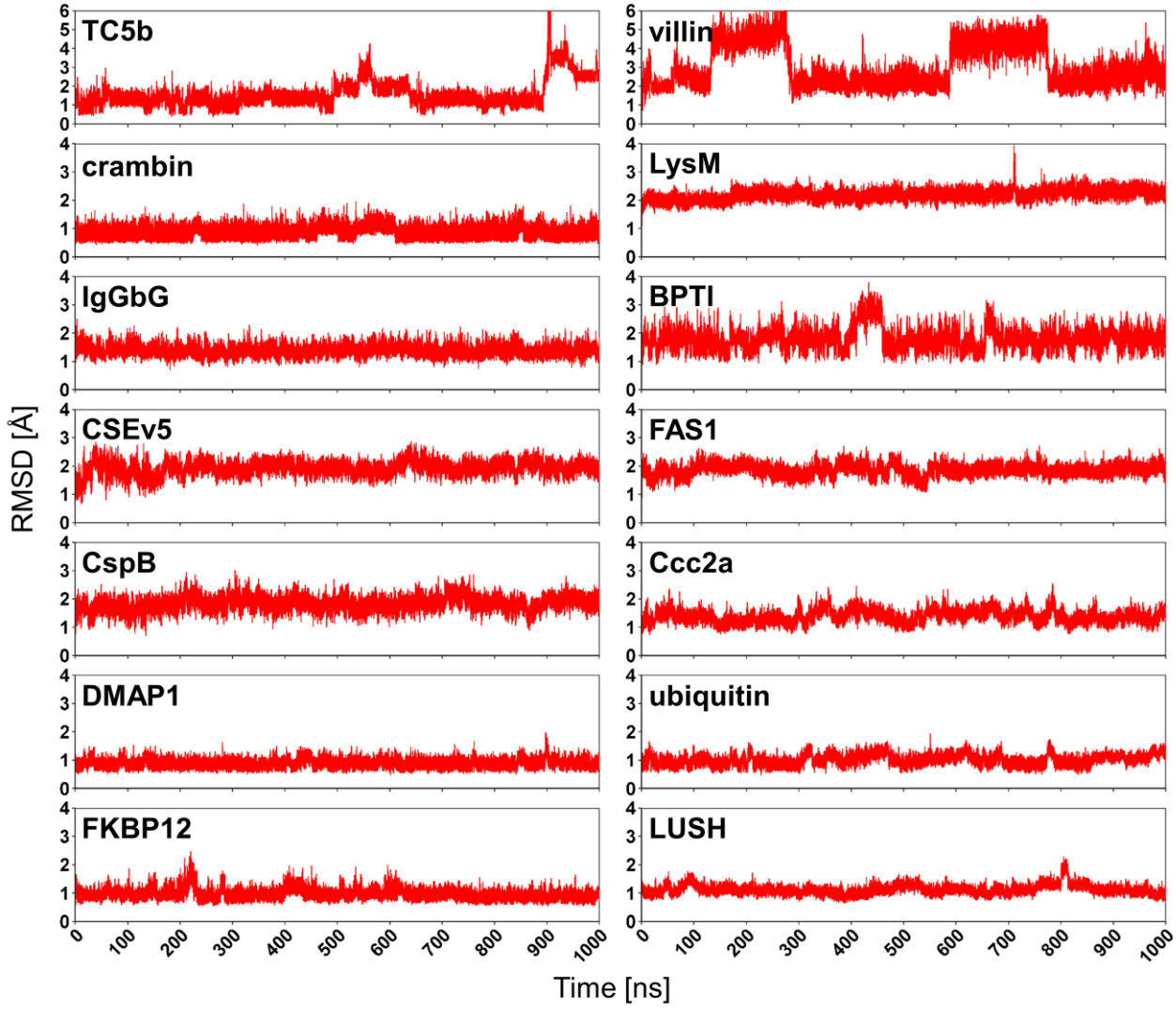

Figure S31. C_α RMSD plots along 1000 ns *ESFF1* simulations for 14 folded proteins.

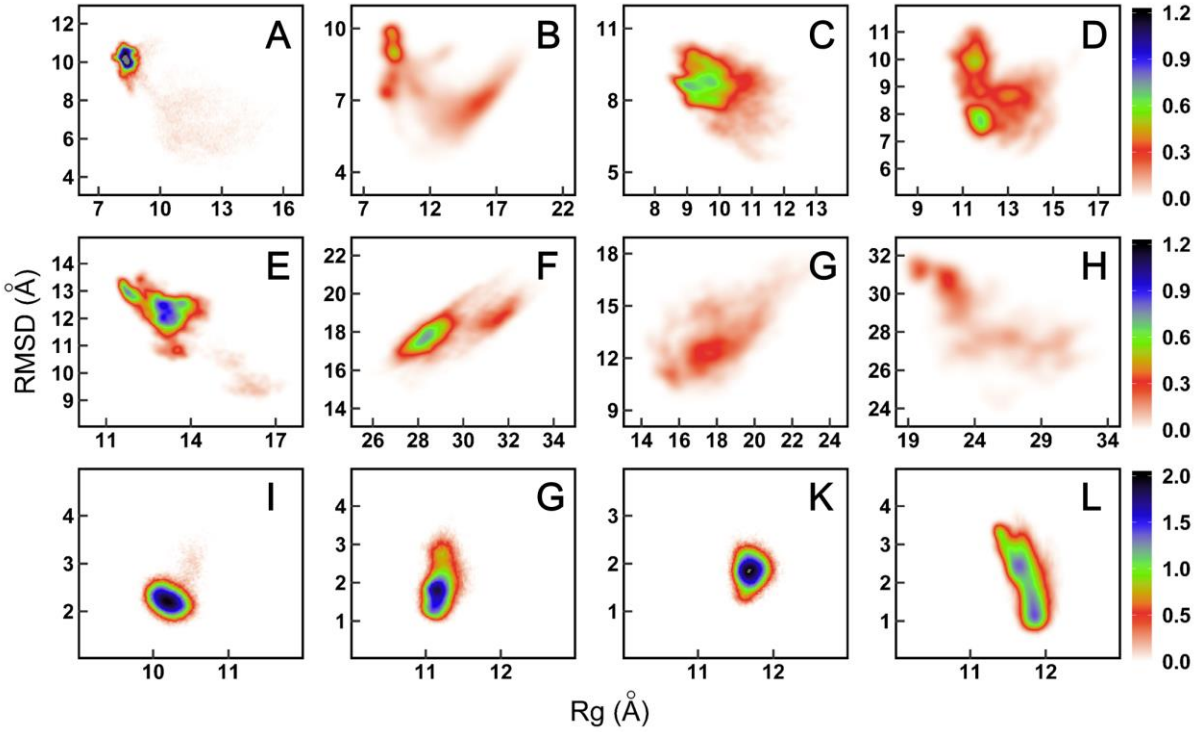

Figure S32. The energy landscape of eight IDPs and four folded proteins in simulations with ESFF1. (A) RS1. (B) C-Myb. (C) MevN. (D) ab40. (E) drkN SH3. (F) ACTR. (G) p53N. (H) α-synuclein. (I) LysM. (J) BPTI. (K) FAS1. (L) ubiquitin.

Table S19. Side-chain J-coupling constants of ubiquitin from *ESFF1* simulations and NMR measurement. The χ_1 represents C'-C_α-C_β-$C_{\gamma1}$, C'-C_α-C_β-$O_{\gamma1}$ and C'-C_α-C_β-$C_{\gamma1}$ dihedral for residues ILE, THR and VAL, respectively. The χ_1' represents C'-C_α-C_β-$C_{\gamma2}$ dihedral for residues ILE, THR and VAL. The standard deviations of J-couplings from the simulations of *ESFF1* force field are given in brackets. The RMSD between the simulated and experimental J-couplings are given in the last row. All units are in Hz.

Residues	**^{3}J(C',C$_\gamma$)**		**^{3}J(N,C$_\gamma$)**	
	Exp.	***ESFF1***	**Exp.**	***ESFF1***
I3-χ_1'	3.68	3.90 (0.00)	0.39	0.43 (0.00)
V5-χ_1	0.00	0.74 (0.00)	1.83	2.10 (0.04)
V5-χ_1'	3.66	3.59 (0.08)	0.46	0.63 (0.04)
T7-χ_1'	2.67	3.58 (0.11)	1.02	0.60 (0.05)
T9-χ_1'	3.00	3.58 (0.05)	0.81	0.57 (0.02)
T12-χ_1'	0.39	0.73 (0.01)	1.61	2.22 (0.01)
I13-χ_1'	1.71	1.14 (0.12)	1.44	2.02 (0.07)
T14-χ_1'	0.76	0.77 (0.02)	1.50	2.07 (0.05)
V17-χ_1	3.93	3.85 (0.01)	0.25	0.45 (0.00)
V17-χ_1'	0.96	0.62 (0.01)	0.68	0.48 (0.00)
T22-χ_1'	3.39	3.79 (0.02)	0.75	0.48 (0.01)
I23-χ_1'	0.94	0.86 (0.01)	2.11	2.10 (0.07)
V26-χ_1'	0.82	0.82 (0.01)	2.16	2.24 (0.00)
V26-χ_1'	4.18	3.86 (0.00)	0.62	0.43 (0.00)
I30-χ_1'	0.96	0.90 (0.00)	2.10	2.24 (0.00)
I36-χ_1'	0.71	0.72 (0.01)	2.08	2.21 (0.03)
I44-χ_1'	0.80	0.88 (0.01)	1.62	2.20 (0.01)
T55-χ_1'	3.02	3.83 (0.01)	0.82	0.54 (0.00)
I61-χ_1'	0.98	0.86 (0.00)	2.15	2.24 (0.00)
V70-χ_1'	2.43	2.63 (0.15)	0.50	0.55 (0.03)
RMSD	**0.41**		**0.32**	

Table S20. RMSD's of secondary chemical shifts between MD simulation and NMR experiment for ACTR-CBP complex.

Protein	Atom	ACTR		CBP	
		ff14SB/TIP3P	*ESFF1/TIP3P*	*ff14SB/TIP3P*	*ESFF1/TIP3P*
free state	C_α	1.288	0.719	0.477	0.409
	C_β	0.575	0.353	0.388	0.395
	C'	1.090	0.634	0.726	0.726
	N	1.912	1.420	1.191	1.144
	H_α	--	--	0.131	0.145
	H_N	0.208	0.178	0.294	0.288
bound state	C_α	0.723	0.731	0.626	0.627
	C_β	0.594	0.430	0.942	1.012
	C'	0.696	0.664	0.597	0.657
	N	2.208	1.618	1.398	1.532
	H_α	0.145	0.116	0.137	0.139
	H_N	0.273	0.218	0.258	0.249

Table S21. RMSD's of secondary chemical shifts between MD simulation and NMR experiment for p53TAD-CBP complex.

Protein	Atom	p53TAD		CBP	
		ff14SB/TIP3P	*ESFF1/TIP3P*	*ff14SB/TIP3P*	*ESFF1/TIP3P*
bound state	C_α	1.248	0.649	0.812	0.725
	C_β	0.697	0.889	0.750	0.791
	C'	0.811	0.400	0.592	0.571
	N	1.326	1.445	1.247	1.199
	H_α	0.106	0.147	0.092	0.087
	H_N	0.219	0.152	0.195	0.180

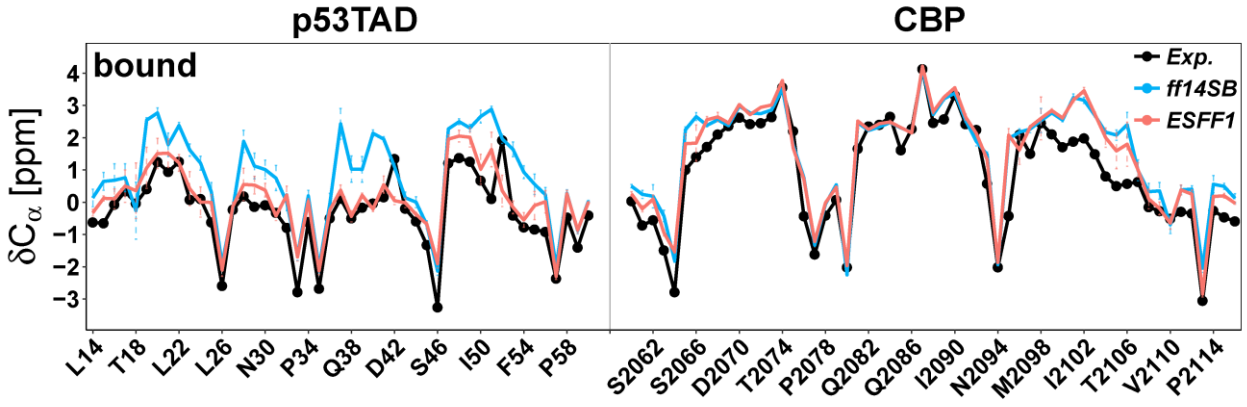

Figure S33. Secondary C_α chemical shift of p53TAD and CBP in bound state in *ff14SB* and *ESFF1* simulations and NMR measurement.

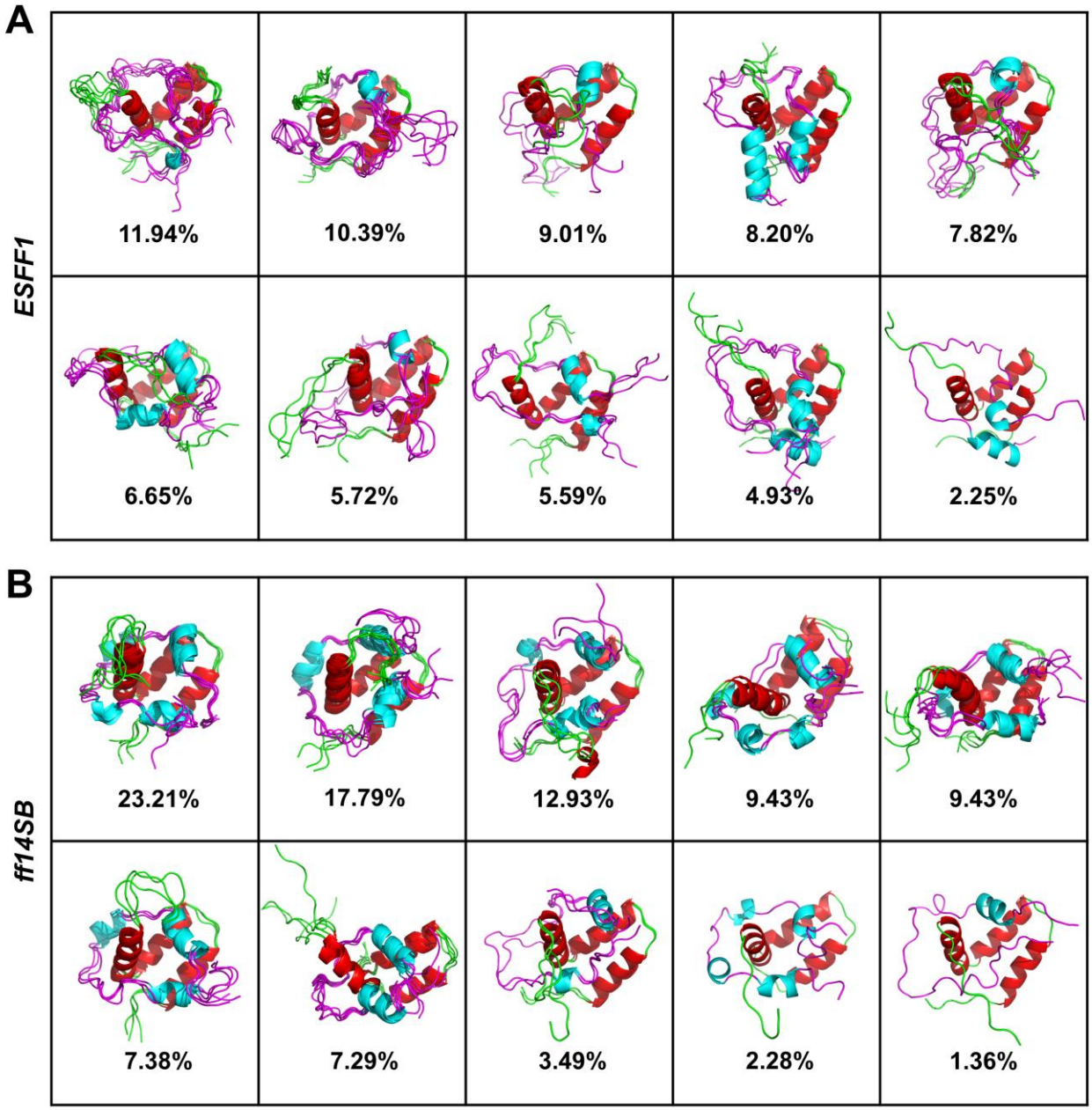

Figure S34. Conformer clusters of CBP-p53TAD protein complex in MD simulations. (A) Dominated conformers and corresponding percentages *ESFF1* simulations. (B) Dominated conformers and corresponding percentages in *ff14SB* simulations.

Table S22. The detailed values of melting curve shown in **Figure 6.**

Proteins		Fraction Folded							
CLN025	Exp.	273 K	275 K	277 K	279 K	281 K	283 K	285 K	287 K
		0.986	0.984	0.982	0.979	0.975	0.972	0.968	0.963
		289 K	291 K	293 K	295 K	297 K	299 K	301 K	303 K
		0.958	0.952	0.945	0.938	0.930	0.921	0.911	0.900
		305 K	307 K	309 K	311 K	313 K	315 K	317 K	319 K
		0.888	0.876	0.862	0.847	0.831	0.814	0.796	0.777
		321 K	323 K	325 K	327 K	329 K	331 K	333 K	335 K
		0.757	0.736	0.714	0.692	0.669	0.645	0.621	0.596
		337 K	339 K	341 K	343 K	345 K	347 K	349 K	351 K
		0.572	0.547	0.522	0.498	0.473	0.450	0.426	0.403
		353 K	355 K	357 K	359 K	361 K	363 K	365 K	367 K
		0.381	0.360	0.339	0.320	0.301	0.283	0.265	0.249
		369 K	371 K	373 K	375 K	377 K	379 K	381 K	383 K
		0.234	0.219	0.205	0.192	0.180	0.168	0.157	0.147
		385 K	387 K	389 K	391 K	393 K	395 K	397 K	399 K
		0.138	0.129	0.120	0.113	0.105	0.099	0.092	0.086
		401 K	403 K	405 K	407 K	409 K	411 K	413 K	415 K
		0.081	0.076	0.071	0.067	0.062	0.059	0.055	0.052
	ESFF1	275 K	285 K	295 K	305 K	315 K	325 K	335 K	345 K
		0.841	0.850	0.839	0.833	0.818	0.807	0.794	0.778
		355 K	365 K	375 K	385 K	395 K	405 K	355 K	365 K
		0.765	0.735	0.689	0.643	0.592	0.522	0.765	0.735
Trizip-2	Exp.	280 K	290 K	300 K	310 K	320 K	330 K	340 K	350 K
		0.91	0.91	0.90	0.87	0.82	0.73	0.58	0.42
		360 K	370 K						
		0.26	0.12						
	ESFF1	280 K	290 K	300 K	310 K	320 K	330 K	340 K	350 K
		0.971	0.956	0.930	0.900	0.877	0.854	0.819	0.788
		360 K	370 K	380 K	390 K	400 K	410 K	420 K	430 K
		0.745	0.685	0.626	0.552	0.442	0.340	0.229	0.159
GB1 hairpin	Exp.	274 K	280 K	286 K	291 K	300 K	310 K	321 K	325 K
		0.850	0.785	0.678	0.581	0.456	0.306	0.196	0.170
		340 K	350 K	359 K					
		0.082	0.047	0.022					

	ESFF1	275 K	285 K	295 K	305 K	315 K	325 K	335 K	345 K
		0.740	0.672	0.563	0.426	0.321	0.252	0.191	0.143
		355 K	365 K	375 K	385 K	395 K	405 K	415 K	425 K
		0.103	0.073	0.060	0.052	0.043	0.032	0.026	0.019
TC5b	**Exp.**	276.329 K	282.243 K	285.979 K	288.780 K	295.006 K	299.987 K	304.033 K	308.080 K
		0.986	0.966	0.939	0.912	0.830	0.759	0.697	0.629
		314.306 K	317.73 K	321.465 K	326.757 K	332.049 K	339.520 K	346.057 K	351.971 K
		0.527	0.476	0.425	0.357	0.296	0.221	0.184	0.146
		358.508 K	364.111 K						
		0.116	0.099						
	ESFF1	275 K	280 K	285 K	290 K	295 K	300 K	305 K	310 K
		0.033	0.039	0.038	0.044	0.043	0.043	0.044	0.043
		315 K	320 K	325 K	330 K	335 K	340 K	345 K	350 K
		0.041	0.039	0.025	0.009	0.007	0.007	0.006	0.005
		355 K	360 K	365 K	370 K	375 K	380 K	385 K	390 K
		0.005	0.005	0.004	0.004	0.004	0.004	0.003	0.003
		395 K	400 K	405 K	410 K	395 K	400 K	405 K	410 K
		0.003	0.002	0.003	0.002	0.003	0.002	0.003	0.002
WW GTT	**Exp.**	288.078 K	292.096 K	298.306 K	303.420 K	309.630 K	314.379 K	322.050 K	328.626 K
		0.995	0.985	0.970	0.960	0.939	0.919	0.889	0.864
		333.374 K	339.219 K	343.968 K	347.986 K	353.100 K	356.753 K	359.311 K	362.233 K
		0.828	0.783	0.737	0.677	0.571	0.480	0.399	0.318
		365.155 K	367.712 K	372.096 K	376.845 K	379.037 K	381.228 K	384.151 K	365.155 K
		0.242	0.177	0.111	0.056	0.035	0.015	0.005	0.242
	ESFF1	280 K	290 K	300 K	310 K	320 K	330 K	340 K	350 K
		0.721	0.618	0.368	0.256	0.144	0.100	0.064	0.042
		360 K	370 K	380 K	390 K	400 K	410 K	420 K	430 K
		0.026	0.017	0.013	0.008	0.006	0.004	0.003	0.002
		440 K	450 K	460 K	470 K				
		0.002	0.001	0.001	0.000				
villin	**Exp.**	280 K	290 K	300 K	310 K	320 K	330 K	340 K	350 K
		1.000	0.999	0.998	0.990	0.967	0.898	0.742	0.500

	ESFF1	360 K	370 K	380 K	390 K	400 K			
		0.269	0.125	0.055	0.024	0.011			
		274 K	282 K	290 K	298 K	306 K	314 K	322 K	330 K
		0.539	0.744	0.833	0.875	0.859	0.839	0.805	0.747
		338 K	346 K	354 K	362 K	370 K	378 K	386 K	394 K
		0.679	0.556	0.419	0.294	0.188	0.114	0.064	0.037
		402 K	410 K	418 K	426 K				
		0.017	0.010	0.005	0.004				

References

(1) Zhang, Y.; Zhou, Y.; He, L.; Fu, Y.; Zhang, W.; Hu, J.; Shi, Z. Hydration Effects on Leu's Polyproline II Population in AcLXPNH2. *Chem Commun (Camb)*. **2018**. *54*, 5764-5767.

(2) Hagarman, A.; Measey, T. J.; Mathieu, D.; Schwalbe, H.; Schweitzerstenner, R. Intrinsic Propensities of Amino Acid Residues in GxG Peptides Inferred from Amide I' Band Profiles and NMR Scalar Coupling Constants. *J Am Chem Soc*. **2010**. *132*, 540-551.

(3) Graf, J.; Nguyen, P. H.; Stock, G.; Schwalbe, H. Structure and Dynamics of the Homologous Series of Alanine Peptides: A Joint Molecular Dynamics/NMR Study. *J Am Chem Soc*. **2007**. *129*, 1179-1189.

(4) Dames, S. A.; Aregger, R.; Vajpai, N.; Bernado, P.; Blackledge, M.; Grzesiek, S. Residual Dipolar Couplings in Short Peptides Reveal Systematic Conformational Preferences of Individual Amino Acids. *J Am Chem Soc*. **2006**. *128*, 13508-13514.

(5) Xiang, S.; Gapsys, V.; Kim, H. Y.; Bessonov, S.; Hsiao, H. H.; Mohlmann, S.; Klaukien, V.; Ficner, R.; Becker, S.; Urlaub, H.; Luhrmann, R.; de Groot, B.; Zweckstetter, M. Phosphorylation Drives a Dynamic Switch in Serine/Arginine-Rich Proteins. *Structure*. **2013**. *21*, 2162-2174.

(6) Raj, P. A.; Marcus, E.; Sukumaran, D. K. Structure of Human Salivary Histatin 5 in Aqueous and Nonaqueous Solutions. *Biopolymers*. **1998**. *45*, 51-67.

(7) Zor, T.; De Guzman, R. N.; Dyson, H. J.; Wright, P. E. Solution Structure of the KIX Domain of CBP Bound to the Transactivation Domain of C-Myb. *J Mol Biol*. **2004**. *337*, 521-534.

(8) Roche, J.; Shen, Y.; Lee, J. H.; Ying, J.; Bax, A. Monomeric Abeta(1-40) and Abeta(1-42) Peptides in Solution Adopt Very Similar Ramachandran Map Distributions That Closely Resemble Random Coil. *Biochemistry*. **2016**. *55*, 762-775.

(9) Marsh, J. A.; Forman-Kay, J. D. Structure and Disorder in an Unfolded State under Nondenaturing Conditions from Ensemble Models Consistent with a Large Number of Experimental Restraints. *J Mol Biol*. **2009**. *391*, 359-374.

(10) Honda, S.; Akiba, T.; Kato, Y. S.; Sawada, Y.; Sekijima, M.; Ishimura, M.; Ooishi, A.; Watanabe, H.; Odahara, T.; Harata, K. Crystal Structure of a Ten-Amino Acid Protein. *J Am Chem Soc*. **2008**. *130*, 15327-15331.

(11) Cochran, A. G.; Skelton, N. J.; Starovasnik, M. A. Tryptophan Zippers: Stable, Monomeric Beta-Hairpins. *Proc Natl Acad Sci U S A*. **2001**. *98*, 5578-5583.

(12) Munoz, V.; Thompson, P. A.; Hofrichter, J.; Eaton, W. A. Folding Dynamics and Mechanism of Beta-Hairpin Formation. *Nature*. **1997**. *390*, 196-199.

(13) Neidigh, J. W.; Fesinmeyer, R. M.; Andersen, N. H. Designing a 20-Residue Protein. *Nat Struct Biol*. **2002**. *9*, 425-430.

(14) Piana, S.; Sarkar, K.; Lindorff-Larsen, K.; Guo, M.; Gruebele, M.; Shaw, D. E. Computational Design and Experimental Testing of the Fastest-Folding Beta-Sheet Protein. *J Mol Biol*. **2011**. *405*, 43-48.

(15) Kubelka, J.; Chiu, T. K.; Davies, D. R.; Eaton, W. A.; Hofrichter, J. Sub-Microsecond Protein Folding. *J Mol Biol*. **2006**. *359*, 546-553.

(16) Zor, T.; Mayr, B. M.; Dyson, H. J.; Montminy, M. R.; Wright, P. E. Roles of Phosphorylation and Helix Propensity in the Binding of the KIX Domain of CREB-Binding Protein by Constitutive (C-Myb) and Inducible (CREB) Activators. *J Biol Chem*. **2002**. *277*, 42241-42248.

(17) Jensen, M. R.; Communie, G.; Ribeiro, E. A., Jr.; Martinez, N.; Desfosses, A.; Salmon, L.; Mollica, L.; Gabel, F.; Jamin, M.; Longhi, S.; Ruigrok, R. W.; Blackledge, M. Intrinsic Disorder in Measles Virus Nucleocapsids. *Proc Natl Acad Sci U S A*. **2011**. *108*, 9839-9844.

(18) Radhakrishnan, I.; Perez-Alvarado, G. C.; Dyson, H. J.; Wright, P. E. Conformational Preferences in the Ser(133)-Phosphorylated and Non-Phosphorylated Forms of the Kinase Inducible Transactivation Domain of CREB. *Febs Lett*. **1998**. *430*, 317-322.

(19) Yamaguchi, T.; Matsuzaki, K.; Hoshino, M. Transient Formation of Intermediate Conformational States of Amyloid-Beta Peptide Revealed by Heteronuclear Magnetic Resonance Spectroscopy. *Febs Lett*. **2011**. *585*, 1097-1102.

(20) Kirkitadze, M. D.; Condron, M. M.; Teplow, D. B. Identification and Characterization of Key Kinetic Intermediates in Amyloid Beta-Protein Fibrillogenesis. *J Mol Biol*. **2001**. *312*, 1103-1119.

(21) Rauscher, S.; Gapsys, V.; Gajda, M. J.; Zweckstetter, M.; de Groot, B. L.; Grubmuller, H. Structural Ensembles of Intrinsically Disordered Proteins Depend Strongly on Force Field: A Comparison to Experiment. *J Chem Theory Comput*. **2015**. *11*, 5513-5524.

(22) Cragnell, C.; Durand, D.; Cabane, B.; Skepo, M. Coarse-Grained Modeling of the Intrinsically Disordered Protein Histatin 5 in Solution: Monte Carlo Simulations in Combination with SAXS. *Proteins*. **2016**. *84*, 777-791.

(23) Granata, D.; Baftizadeh, F.; Habchi, J.; Galvagnion, C.; De Simone, A.; Camilloni, C.; Laio, A.; Vendruscolo, M. The Inverted Free Energy Landscape of an Intrinsically Disordered Peptide by Simulations and Experiments. *Sci Rep*. **2015**. *5*, 15449.

(24) Choy, W. Y.; Mulder, F. A.; Crowhurst, K. A.; Muhandiram, D. R.; Millett, I. S.; Doniach, S.; Forman-Kay, J. D.; Kay, L. E. Distribution of Molecular Size within an Unfolded State Ensemble Using Small-Angle X-Ray Scattering and Pulse Field Gradient Nmr Techniques. *J Mol Biol*. **2002**. *316*, 101-112.

(25) Yang, J.; Yan, R.; Roy, A.; Xu, D.; Poisson, J.; Zhang, Y. The I-TASSER Suite: Protein Structure and Function Prediction. *Nat Methods*. **2015**. *12*, 7-8.

(26) Kjaergaard, M.; Norholm, A. B.; Hendus-Altenburger, R.; Pedersen, S. F.; Poulsen, F. M.; Kragelund, B. B. Temperature-Dependent Structural Changes in Intrinsically Disordered Proteins: Formation of Alpha-Helices or Loss of Polyproline II? *Protein Sci*. **2010**. *19*, 1555-1564.

(27) Schwalbe, M.; Ozenne, V.; Bibow, S.; Jaremko, M.; Jaremko, L.; Gajda, M.; Jensen, M. R.; Biernat, J.; Becker, S.; Mandelkow, E.; Zweckstetter, M.; Blackledge, M. Predictive Atomic Resolution Descriptions of Intrinsically Disordered Htau40 and Alpha-Synuclein in Solution from NMR and Small Angle Scattering. *Structure*. **2014**. *22*, 238-249.

(28) Morar, A. S.; Olteanu, A.; Young, G. B.; Pielak, G. J. Solvent-Induced Collapse of Alpha-Synuclein and Acid-Denatured Cytochrome C. *Protein Sci*. **2001**. *10*, 2195-2199.